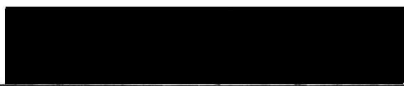# AN ABSTRACT OF THE THESIS OF

GARY LAMONT UPHAM for the MASTER OF SCIENCE
(Name)   (Degree)

in NUCLEAR ENGINEERING presented on December 11, 1967
(Major)   (Date)

Title: FLUX MEASUREMENTS IN THE OREGON STATE TRIGA

REACTOR

Abstract approved: ▮▮▮▮▮▮▮▮▮▮▮▮
John C. Ringle

Neutron flux and gamma-ray dose have been measured in the experimental facilities of the Oregon State TRIGA reactor.

Thermal neutron flux measurements utilized foil activation techniques.

The gamma-ray dose was measured with a thermoluminescent dosimetry system. The thermoluminescent material used was LiF.

Fast neutron spectrum measurements were performed. The fast flux measurements utilized threshold detectors. The activation data from the various threshold detectors was analyzed using the Effective Threshold Method. Fast flux measurements were made only in the in-core and near-core experimental facilities (where a fission spectrum was assumed to exist).

Flux Measurements in the Oregon State
TRIGA Reactor

by

Gary Lamont Upham

A THESIS

sumbitted to

Oregon State University

in partial fulfillment of
the requirements for the
degree of

Master of Science

June 1968

APPROVED;

Professor of Mechanical and Industrial Engineering
in charge of major

Head of Department of Mechanical and Industrial
Engineering

Dean of Graduate School

Date thesis is presented _December 11, 1962_

Typed by Clover Redfern for ___Gary Lamont Upham___

TABLE OF CONTENTS

LIST OF TABLES

LIST OF FIGURES

FLUX MEASUREMENTS IN THE OREGON STATE
TRIGA REACTOR

INTRODUCTION

Statement of the Problem

Measurement of neutron and gamma-ray fluxes in the experimental facilities of the Oregon State TRIGA[1] Reactor (OSTR) has been performed. While the various TRIGA reactors are somewhat standardized, they all differ in some respects. Experimental measurements of neutron and gamma fluxes are required to determine precisely what neutron and gamma fluxes will be encountered in a given facility.

This work was undertaken to provide information for future experimenters regarding neutron and gamma-ray fluxes in the various TRIGA facilities.

Method of Attack

Foil activation is a common and well known method for measuring thermal neutron flux. The experimental tools needed to perform the measurement are a minimum: detector foils, and a gamma-ray scintillation counter or proportional counter. Thus it was decided

---

[1]Abbreviation for Training, Research, Isotope, General Atomic.

that for the large number of measurements to be made that the foil method of thermal neutron measurement would be used.

There are a number of ways to measure gamma dose. These include ionization chambers, glass dosimeters and thermoluminescent dosimeters. The thermoluminescent dosimetry system is attractive from the standpoint of low cost (dosimeters are reusable), the ability to measure a wide range of doses, small size, remote use, and general ease of use. Thermoluminescent dosimetry was chosen for measurement of gamma-ray dose.

It also was desired to measure the fast neutron spectrum (the neutron flux as a function of energy) in the core region of the reactor. Threshold detectors are widely used to measure fast neutron spectra. A threshold reaction requires a neutron of energy equal to or greater than the threshold energy to initiate the reaction. By using a number of threshold detectors with differing threshold values, the neutron spectrum can be ascertained. The threshold detector technique also requires a minimum of equipment: various threshold detector materials and a suitable gamma-ray scintillation counter.

The technique and theory of utilizing these three methods and the results obtained from their use are discussed in the following sections.

DESCRIPTION OF REACTOR

General Description

The Oregon State University TRIGA Mark II reactor (OSTR) is a heterogeneous swimming pool-type reactor. The core utilizes a solid homogeneous fuel-moderator element, developed by General Atomic, in which the zirconium hydride moderator is homogeneously combined with 20 percent enriched (in U^{235}) uranium. The unique feature of these fuel-moderator elements is the prompt negative temperature coefficient of reactivity which allows the TRIGA to be operated in the pulsing mode. The reactor is also moderated and cooled by demineralized water. The principal areas of utilization of the reactor are isotope production, training, and research. Presently the maximum steady state power is 250 kw, while maximum power achieved (momentarily) during pulsing is on the order of 1200 mw.

Reactor Structure

The structure of the OSTR, shown in Figures 1 and 2, consists of a concrete shield containing an aluminum reactor tank. The reactor core is located near the bottom of the tank, which is approximately 6-1/2 feet in diameter and 20-1/2 feet in depth. The core is shielded radially by approximately 1-1/2 feet of water and 8 feet 2 inches concrete, and vertically by approximately 16 feet of
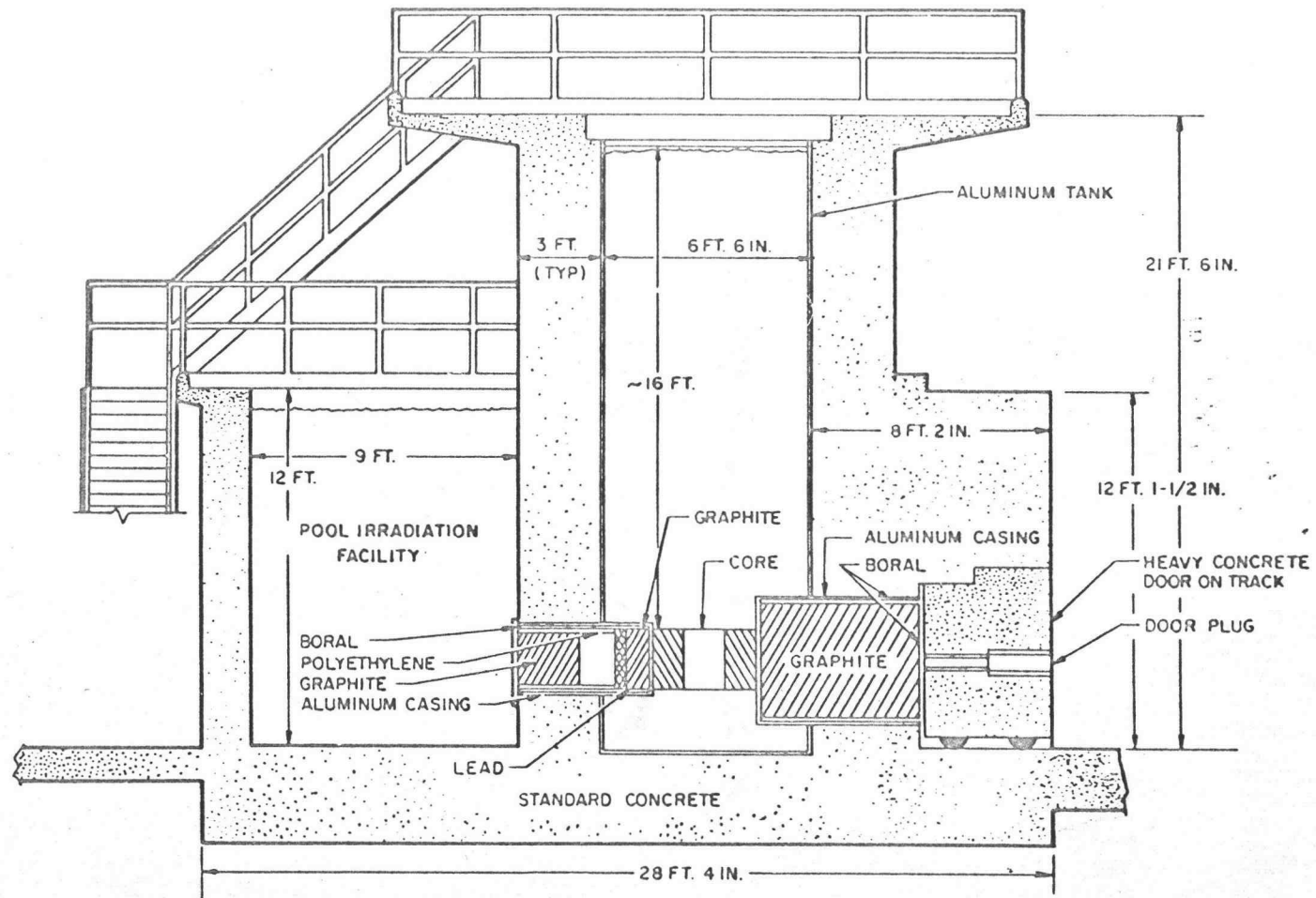
Figure 1. Vertical section view of reactor.
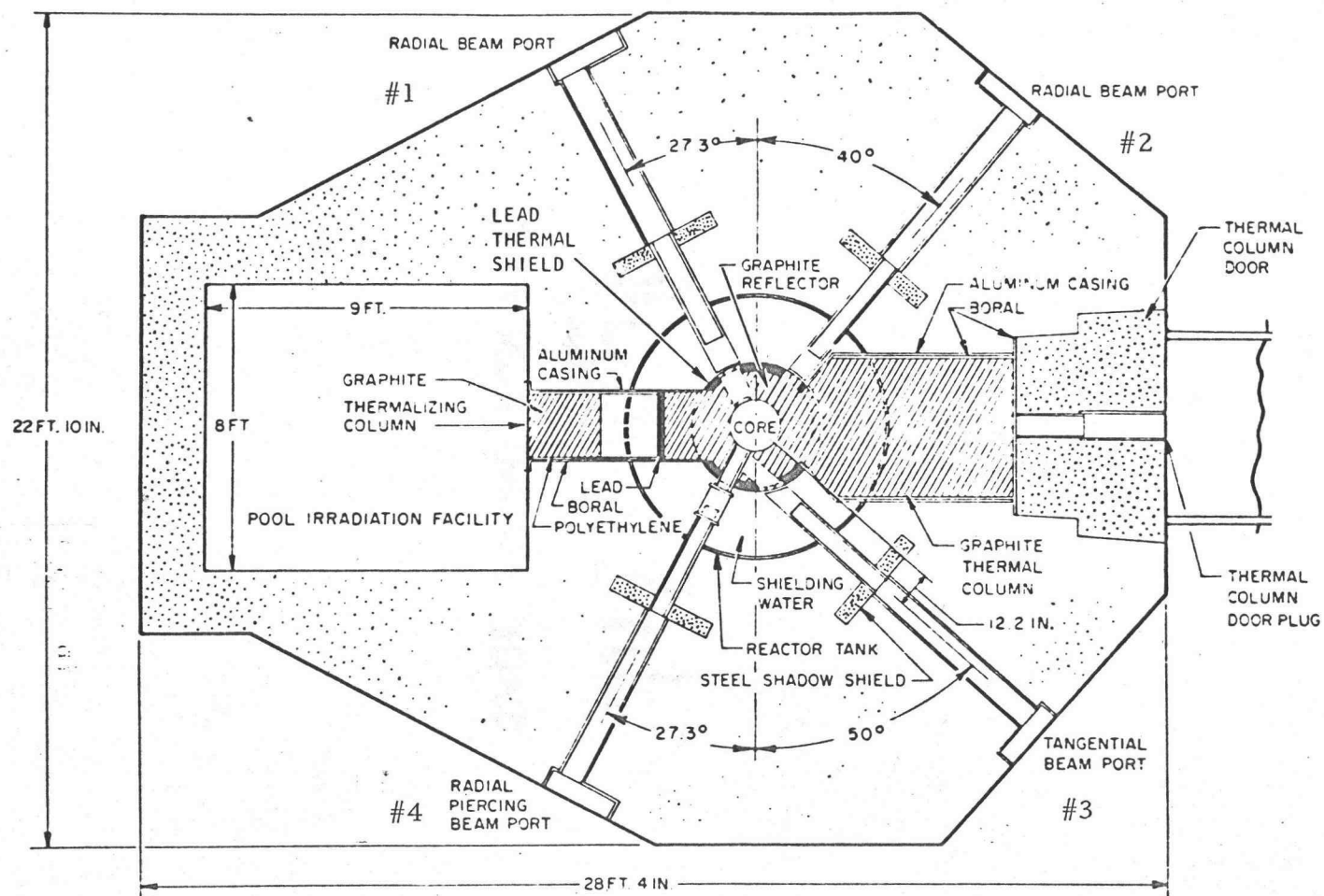
Figure 2. Horizontal section view of reactor.

demineralized water. Four 6-inch diameter beam tubes and a 4 by 4 by 5-1/2 foot graphite thermal column (see Figure 2) penetrate the concrete shield and reactor tank. A 2 by 2 by 4.3 foot graphite themalizing column penetrates the concrete shield and terminates in a bulk-shielding experimental tank that is part of the shielding structure (see Figures 1 and 2).

Reactor Core

The core loading of the OSTR used during this investigation is shown in Figure 4. The reactor core is a right circular cylinder consisting of cylindrical fuel-moderator elements and graphite dummy elements. Water occupies approximately one-third of the core volume. The critical loading of the core was 59 fuel-moderator elements. The present loading is 70 fuel-moderator elements, which includes two fuel followers on two control rods. There are three control rods, utilizing graphite impregnated with powdered boron carbide as the neutron absorber. The regulating and shim rods have fuel followers, while the transient rod has an air follower.

The core components are contained between top and bottom aluminum grid plates. The top grid plate has 126 positions for fuel elements, control rods, etc. They are arranged, as shown in Figure 4, in six concentric rings around a central thimble to be used for high flux irradiations.

Neutron reflection in the radial direction is provided by about ten inches of graphite contained in an aluminum container 29 inches high. Also in this container, at the outer perimeter, there are two inches of lead which acts as a thermal shield to protect the concrete structure from excessive nuclear heating; the lead also contributes to reducing the dose outside the concrete shield. The core arrangement is shown in Figure 3. Four instrumentation channels monitor and indicate the neutron flux and power level and their rate of change. One fuel moderator element in the "B" ring of the core is instrumented with thermocouples to record fuel temperature.

The active part of each fuel-moderator element is approximately 1.5 inches in diameter and 15 inches long. The fuel "meat" is about 8-1/2 percent by weight of uranium enriched to 20 percent in U^{235}. The hydrogen-to-zirconium atom ratio is approximately 1.7 to 1.0. Each element is clad with a 0.020-inch-thick stainless steel can. Two 3.5-inch sections of graphite are inserted in the can, one above and one below the fuel, to serve as top and bottom reflectors for the core. The approximate over-all weight of the element is 7.5 pounds; the U^{235} content ranges from about 36 to 40 grams.

Irradiation Facilities

The TRIGA Mark II system is designed to provide intense fluxes of ionizing radiation for research, training, and isotope production.
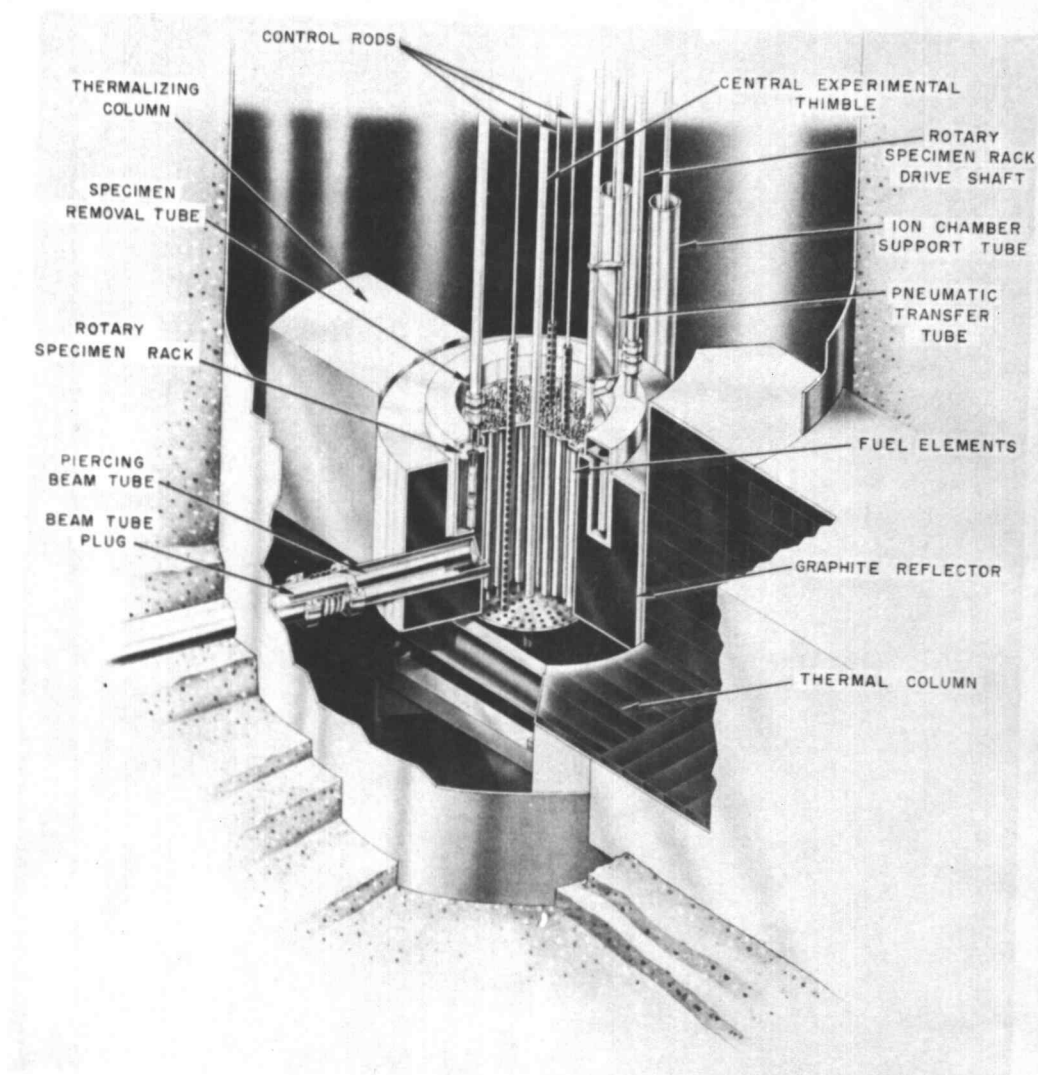
Figure 3. Cutaway view of standard TRIGA Mark II core arrangement.
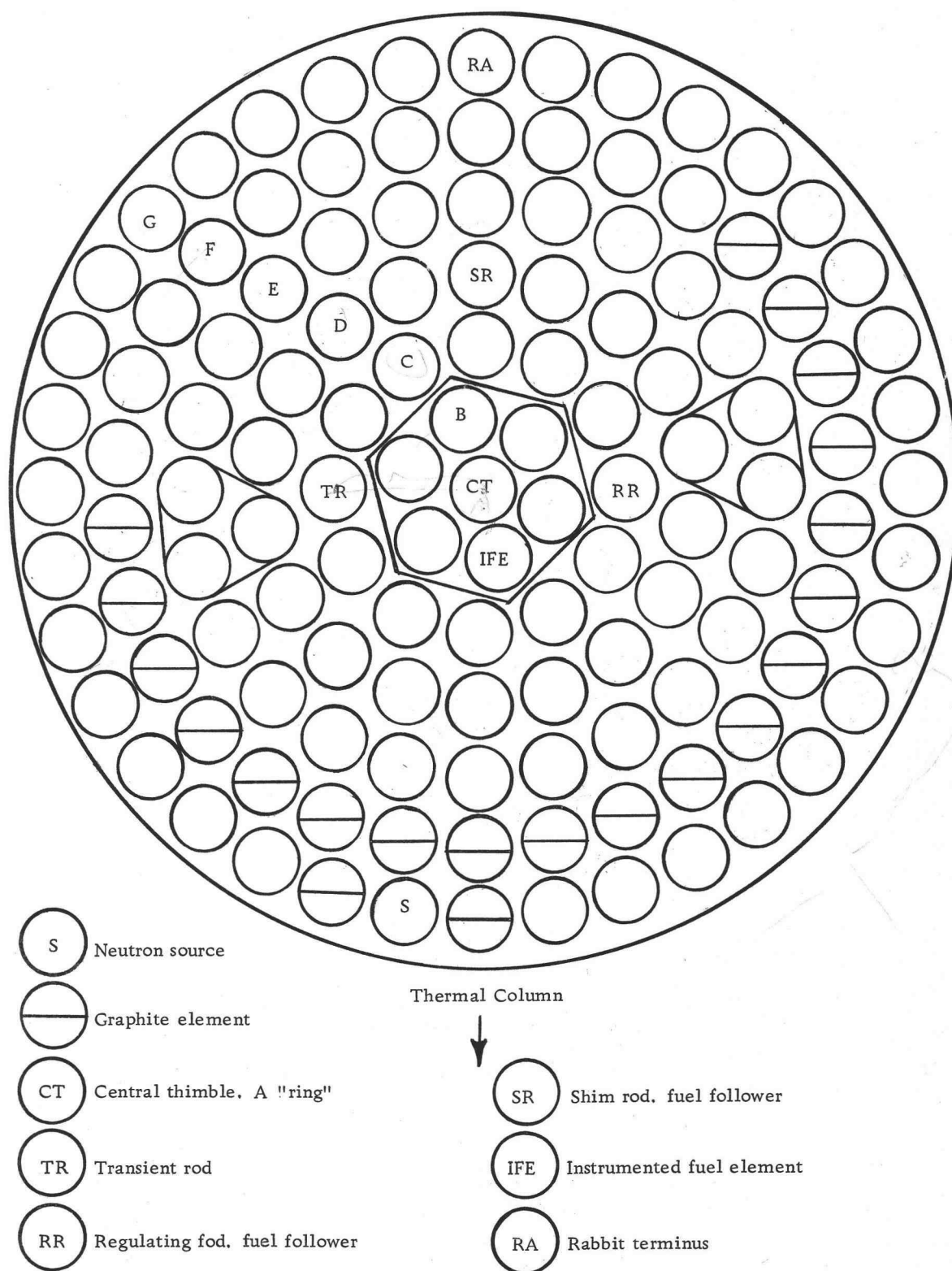
Figure 4. Core loading of OSTR.

Experiments or irradiations with the TRIGA reactor can be carried out primarily in conjunction with the following facilities:

1. Isotope - production facility,

2. Pneumatic transfer system,

3. Central thimble,

4. Beamport facilities,

5. Thermal column,

6. Thermalizing column and bulk shielding experimental tank,

7. In-pool (above reactor) and in-core irradiation facilities.

It is believed that a compilation of results will be most useful if it is arranged according to a specific facility, rather than listing, for example, the results of all gamma dose measurements for all facilities in a single section.

The compilation of results will be arranged thusly: a brief description of pertinent information about a given facility will preceed the listing of results for that facility.

Due to the similarity or proximity of some facilities, they have been grouped in three major divisions: (1) in core and near core facilities, (2) beam ports, (3) thermal column and thermalizing column/bulk irradiation pool.

If the reader requires a more detailed description of any given facility, the OSTR blue prints and/or the OSU TRIGA manual should be consulted.

EXPERIMENTAL RESULTS

In-Core and Near-Core Facilities

The in-core and near-core facilities include the central thimble, isotope production facility, and pneumatic transfer system. Figure 3 gives a clear picture of the position of these facilities. Figure 4 shows the location of the central thimble and rabbit terminus in the core. Table 1 includes a summary of the neutron and gamma fluxes found in the in-core and near-core facilities.

Isotope Production Facility

The isotope production facility consists of the rotary specimen rack, located in a circular well in the reflector assembly, and the associated equipment used for introducing specimens into the rotating rack. The rotating rack supports 40 evenly-spaced tubular aluminum containers, which serve as receptacles for specimen containers. Plastic irradiation specimen containers, known as "TRIGA tubes," made of polystyrene are used exclusively in the rotating rack for containing specimens to be irradiated in this facility. The usable space in each TRIGA tube is 0.81 inch in diameter by 3.81 inches long, which is equivalent to about 2.0 cubic inches. Two TRIGA tubes can be inserted in each rotary specimen rack position.

The thermal neutron flux was measured in the rotary specimen

Table 1. Summary of neutron and gamma measurements, 250 KW.

Facility	Thermal neutron flux, n/cm^2-sec	R_{cd} (foil material)	γ dose R/hr	Relative fast neutron flux, $E > 1.7$ Mev (ϕ central thimble = 1.0)
Rabbit (max.)	$2.2 \pm .4 \times 10^{12}$	3.02 (Au)	$2.0 \pm .3 \times 10^7$	.087
Central thimble (max.)	$5.5 \pm 1.1 \times 10^{12}$	1.6 (Au) 8.2 (Mn)	$1.0 \pm .3 \times 10^8$	1.0
Rotating rack (max.)	$6.6 \pm 1.9 \times 10^{11}$	3.06 (Au)	$1.25 \pm .2 \times 10^7$	.028
Beam port #1 (inner end)	$(1.0 \pm .2) \times 10^{11}$	18.5 (Au)	$(2.8 \pm .3) \times 10^6$	.016
Beam port #2 (inner end)	$(4.6 \pm .9) \times 10^{10}$	20.4 (Au)	$(1.5 \pm .15) \times 10^6$	.0037
Central stringer thermal column (inner end)	$(5.1 \pm 1.0) \times 10^{10}$	243 (Mn) 43 (Au)	$(2.0 \pm .2) \times 10^5$	---
Pool irradiation facility ($\mathbb{C_L}$ thermalizing column)	$(3.85 \pm .8) \times 10^8$	52 (Au)	$(1.54 \pm .2) \times 10^3$	---

rack with two TRIGA tubes in one container. The results are shown in Figure 5. The gamma dose was measured in a similar manner, and the results are shown in Figure 6. In both cases the rack was rotating during irradiation. The fast neutron flux spectrum as measured in the rotating rack is shown in Figure 7.

Pneumatic Transfer System

The pneumatic transfer system is a very convenient and rapid means of irradiating samples in a high flux region. The terminus of the pneumatic transfer system as shown in Figure 4, is in the "G" ring of the core grid plate, it is thus outside the active core (fuel) region. The pneumatic transfer system rapidly conveys a specimen to and from the reactor core. The low transit time (approximately five seconds in or out) is important in the utilization of very short-lived isotopes. The system is controlled from the receiving area and may be operated either manually or automatically, i.e., with an electric timing device incorporated into the system so that the specimen capsule is ejected automatically from the core after a predetermined length of time. Four solenoid-operated valves control the air flow. The system operates on a pressure differential, drawing the specimen capsule into and out of the core by vacuum. The pneumatic transfer system derives the name "rabbit" from the specimen capsule made of polyethylene that is used to convey samples in and out of
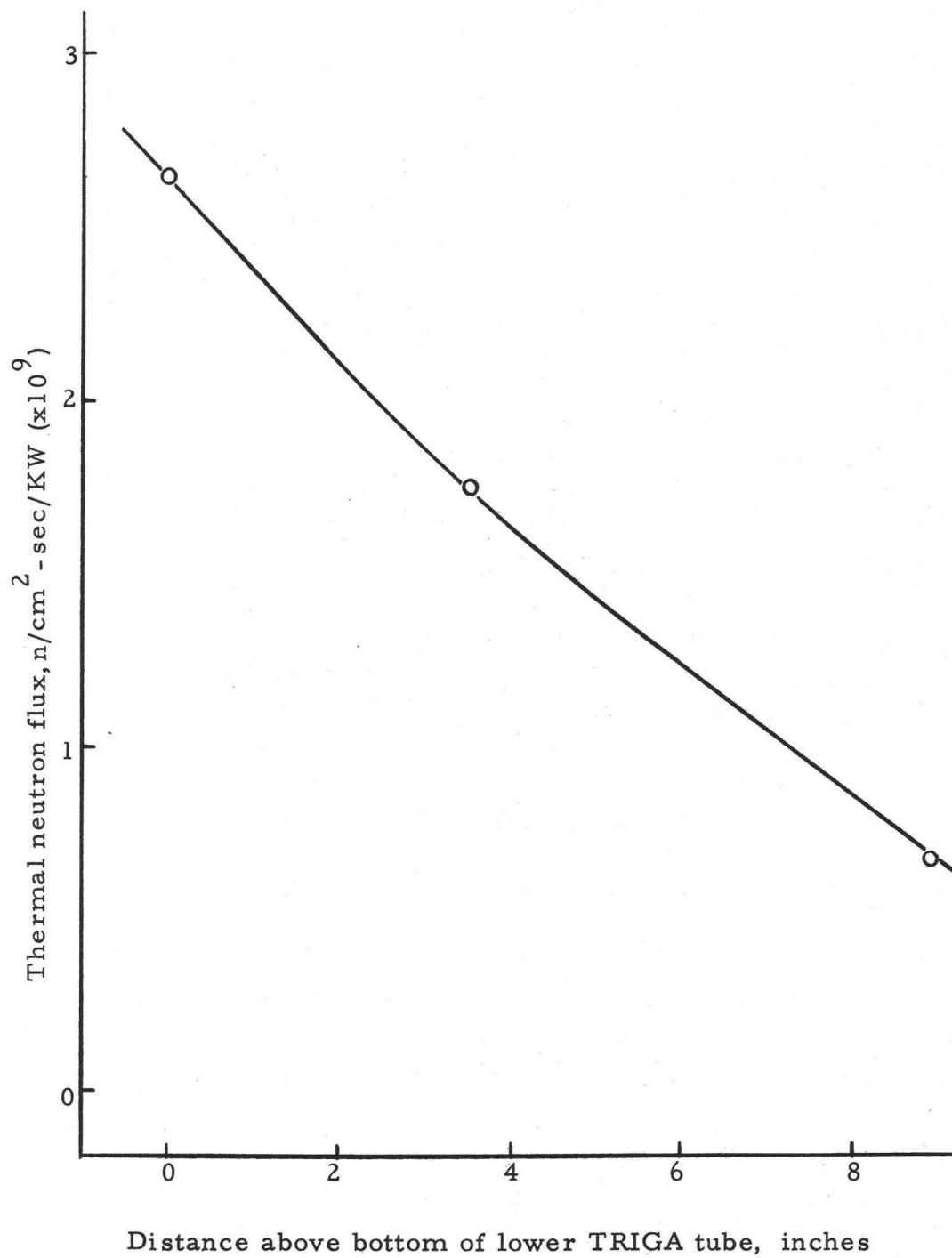
Figure 5. Thermal neutron flux, rotating specimen rack.
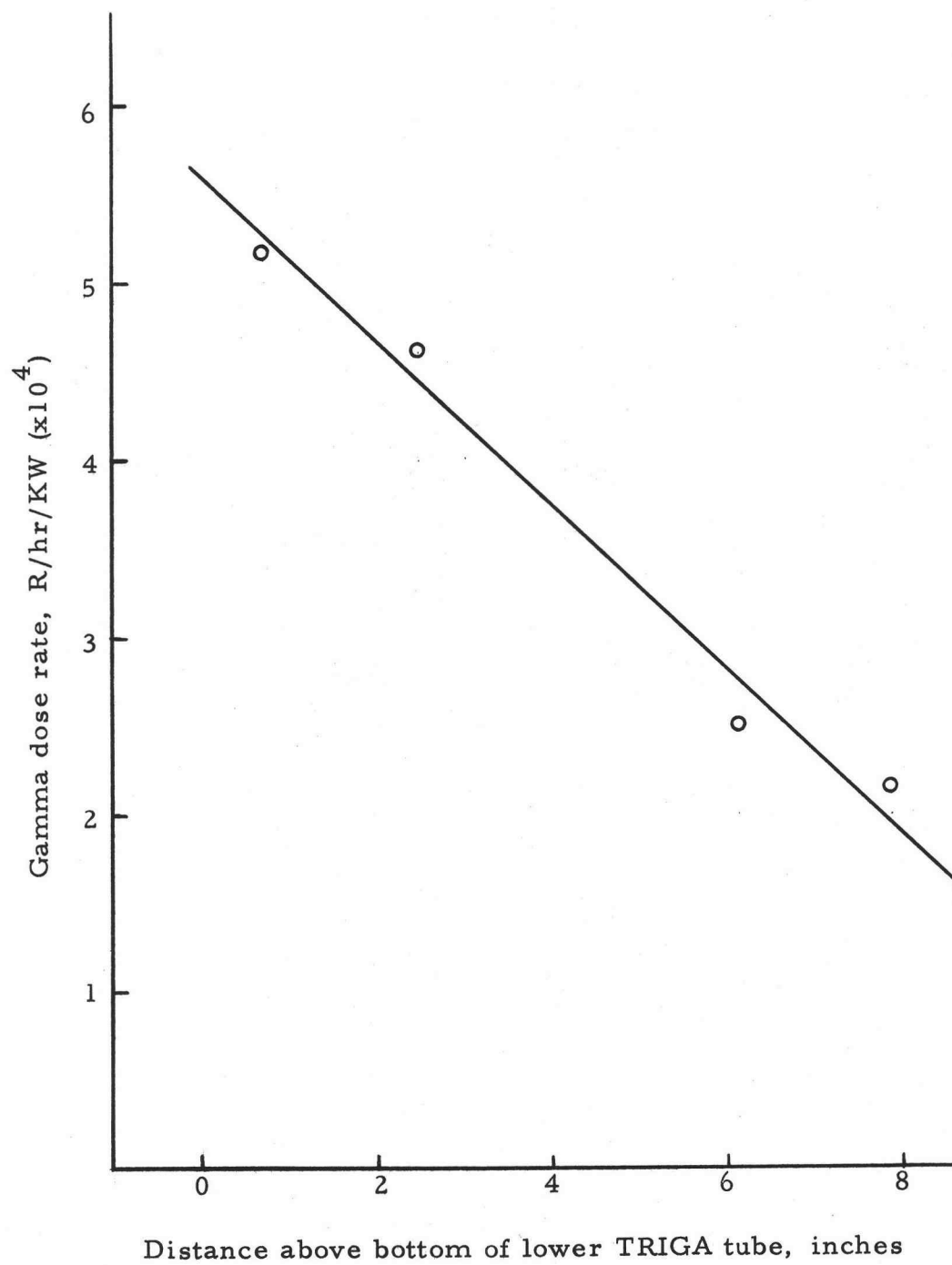
Figure 6. Gamma dose rate rotating specimen rack.
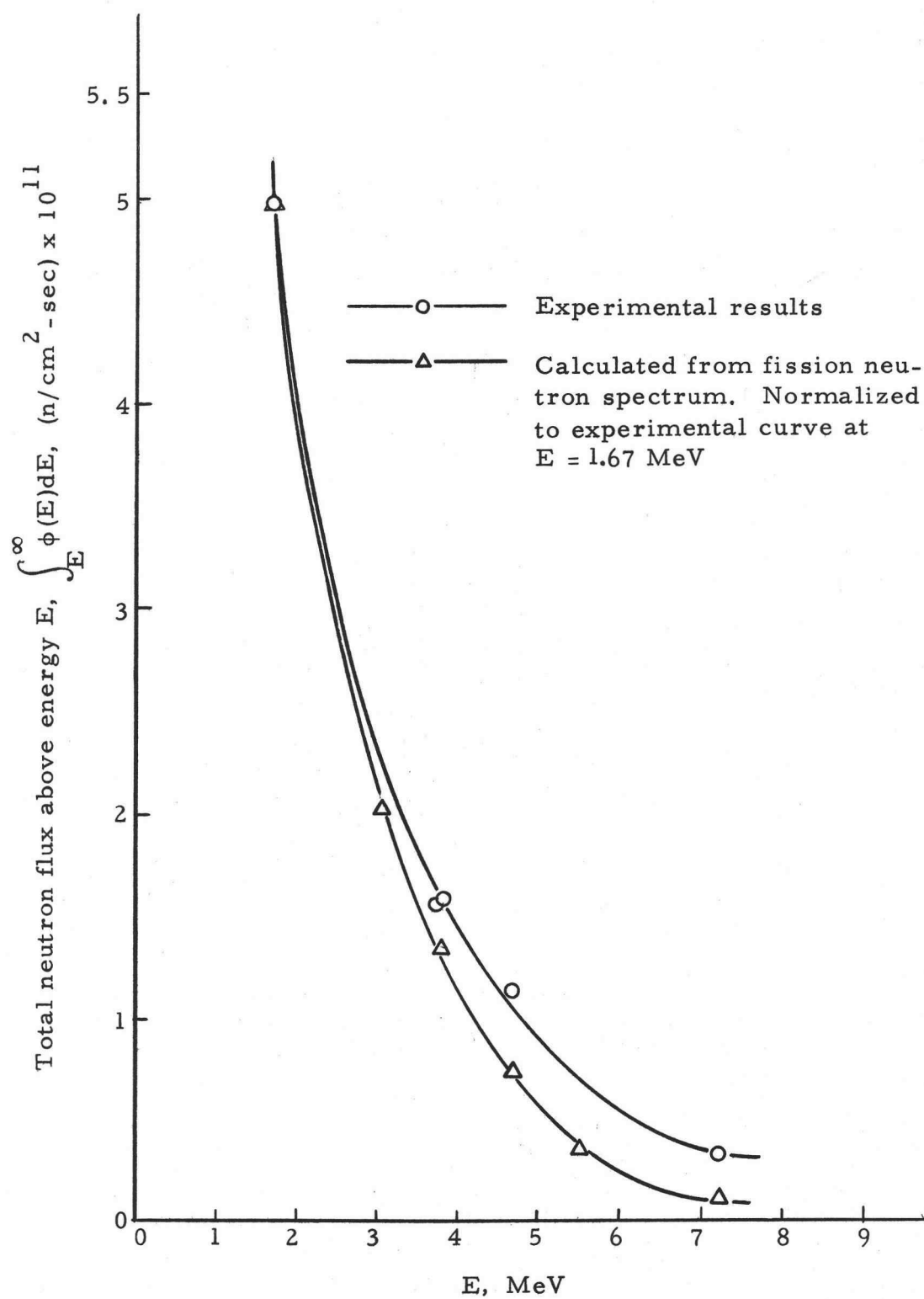
Figure 7. Fast neutron flux, rotating rack, 250KW.

the core. The inner dimensions of the capsule are 0.68 inch in diameter by 4.5 inches in length.

The thermal neutron flux, and gamma dose measurements for the rabbit are listed in Table 1. These values are for the bottom (maximum neutron flux and gamma dose point) of the rabbit while in the reactor. The neutron flux and gamma dose vary slightly (decrease) going from the bottom to the top of the inside of the rabbit. The linearity of the power level, as read from the linear power recorder on the console, was determined as a function of neutron flux. The power level, as a function of neutron flux, as shown in Figure 8, is quite linear as would be expected. The fast neutron spectrum as measured in the rabbit is shown in Figure 9.

Central Thimble

The central thimble, located in the center of the core, provides space for the irradiation of small samples at the point of maximum flux. It also makes possible the extraction of a highly collimated beam of neutron and gamma radiation.

The central thimble is an aluminum tube 1-1/2 inches in outside diameter with a wall thickness of 0.083 inch. It extends from the bridge above the reactor tank straight down through the core. Air pressure is applied to force the shielding water out of the central thimble to create a neutron and gamma beam.
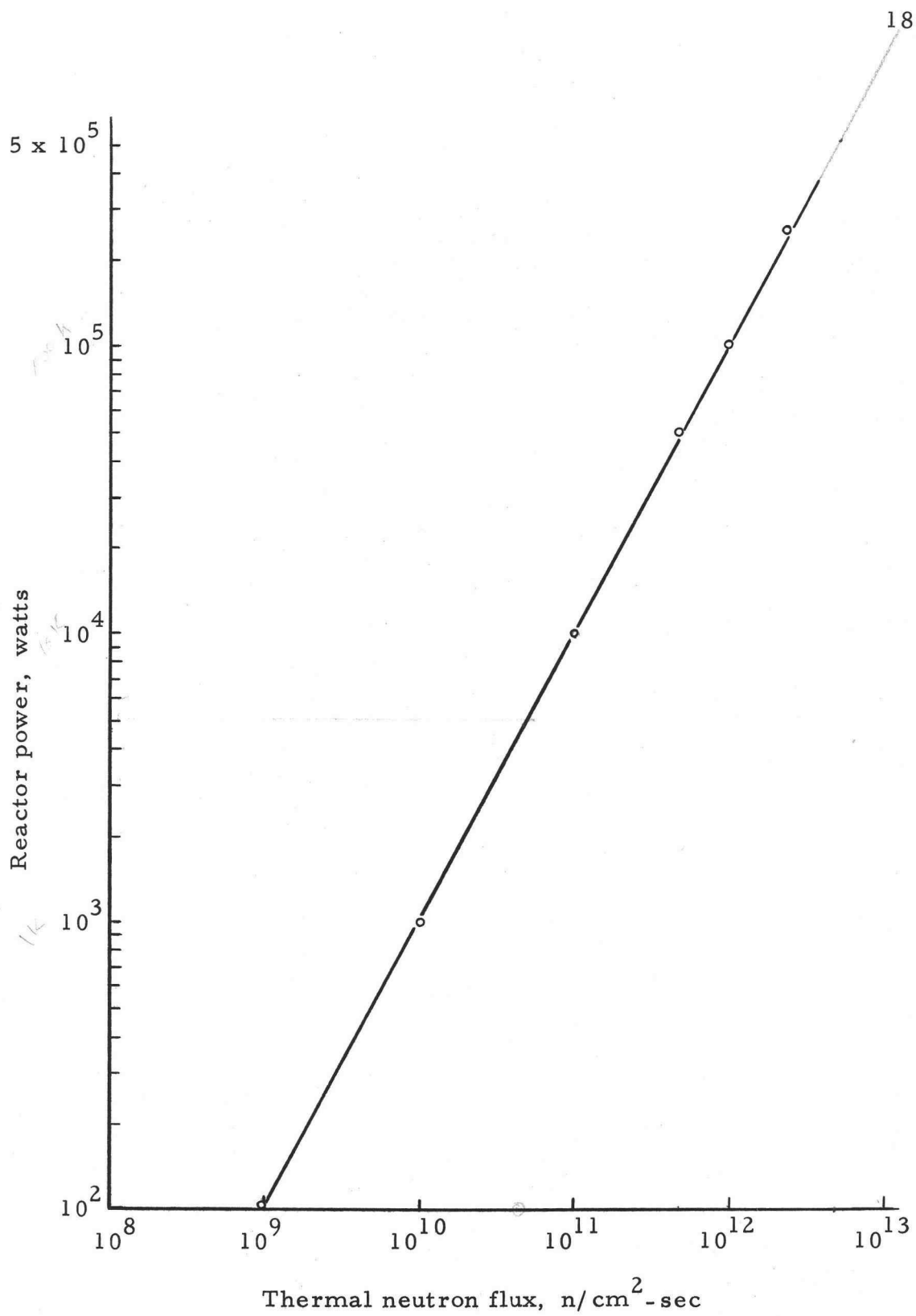
Figure 8. Reactor power as a function of thermal neutron flux in the rabbit facility.
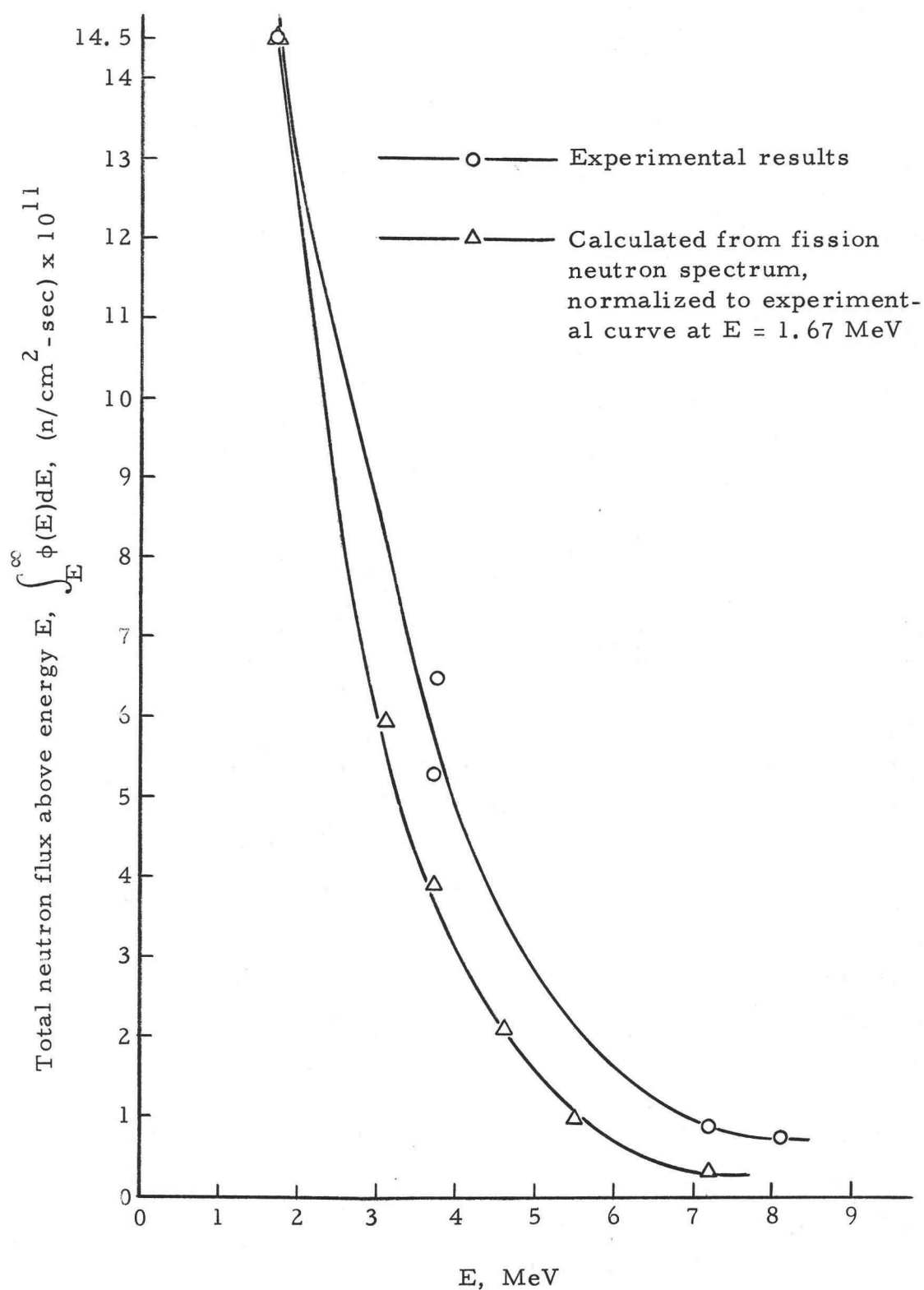
Figure 9. Fast neutron flux, pneumatic transfer facility,
250 KW.

The thermal neutron flux and gamma dose were measured in the central thimble (water filled). The neutron flux is plotted in Figure 10. The gamma dose is plotted in Figure 11. The flux was measured along the vertical axis of the central thimble, and hence along the vertical axis of the core. The horizontal centerline of the core is used as a reference point. It is seen from Figure 10 that the neutron flux is not symmetrical about the centerline of the core in the central thimble. This is no doubt due to the presence of the three neutron absorbing control rods, which have perturbed the neutron flux (and to a much lesser extent the gamma dose). The control rods were all held at approximately 600 units, as read at the reactor console, during the irradiations in the central thimble. The fast neutron spectrum in the central thimble, as measured at the core centerline, is shown in Figure 12.

Beam Port Facilities

The four beam ports, as shown in Figure 2, penetrate the concrete shield and the aluminum tank and pass through the reactor tank water to the reflector. These ports provide beams of neutron and gamma radiation. Specimens up to six inches in diameter may be irradiated in a region close to the core. Three of the beam ports are oriented radially with respect to the center of the core, and a fourth port is tangential to the outer edge of the core. Two of the radial
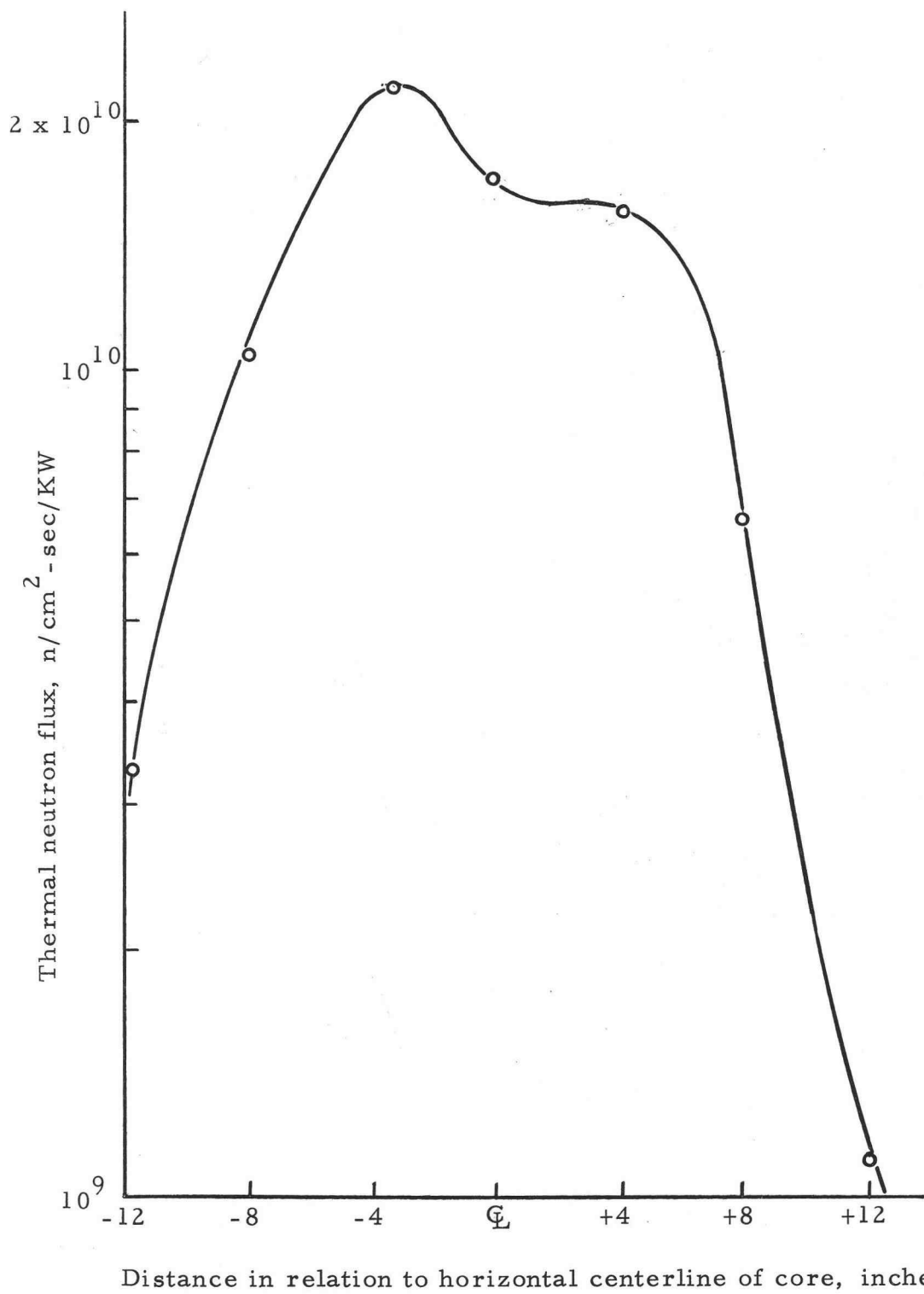
Figure 10.   Thermal neutron flux, central thimble, water filled.
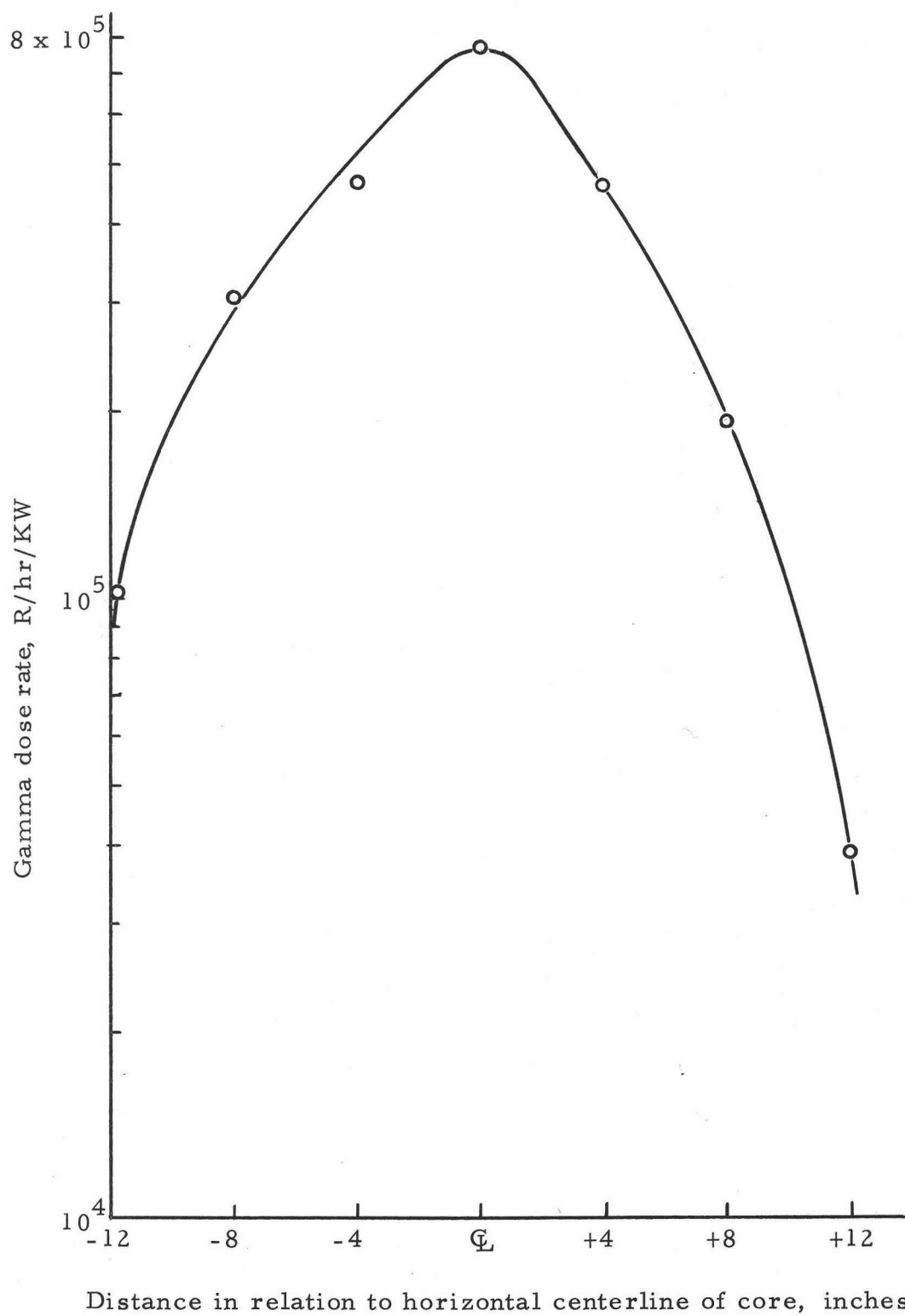
Figure 11. Gamma dose rate, central thimble.
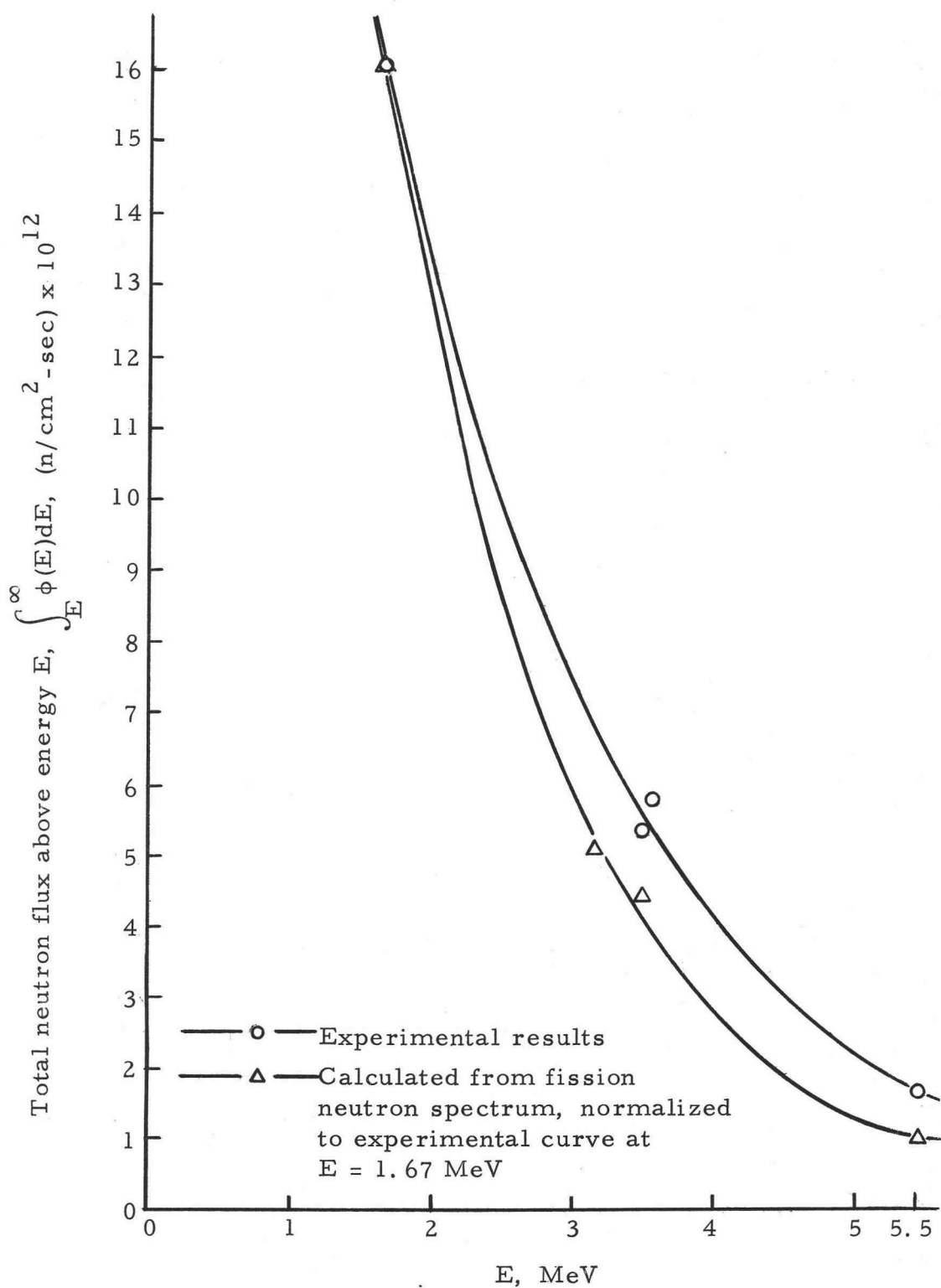
Figure 12. Fast neutron flux, central thimble 250 KW.

tubes terminate at the outer edge of the reflector assembly (B. P. #'s

1 and 2); one of these is aligned with a cylindrical void in the reflector

graphite (B. P. #1). The third radial (or piercing) port (B. P. #4)

penetrates into the graphite reflector and terminates at the inner sur-

face of the reflector assembly, just at the outer edge of the core. In

order to have the beam port voids in the reflector graphite pass be-

neath the rotary specimen rack, their horizontal centerlines are lo-

cated 2-3/4 inches below the centerline of the core.

The tangential beam port (B. P. #3) terminates at the outer sur-

face of the reflector, but is also aligned with a cylindrical void,

which intersects the piercing tube in the reflector graphite. This

tangential port provides a radiation source giving a minimum amout

of core gamma radiation.

To prevent radiation streaming through the gap between the

beam tube and the inner shielding plug, a step is incorporated in the

beam tube. The outer section (furthest from the core) of the beam

tube has a nominal diameter of eight inches, while the inner section

has a six-inch diameter. The inner beam plug provides shielding

while the beam port is not being utilized.

Due to radiological problems (excessive dose rates in unre-

stricted areas) the inner end of the inner beam plug was not pulled

out of the six-inch diameter section of the beam tube. If the plug was

pulled past the step in the tube, there was radiation streaming

necessitating very low power levels, inadequate for proper activation of detector foils. Leaving the inner plug partially in the six inch section of the beam tubes reduced the length of the beam port available for flux mapping to about 40 inches.

Foils and LiF capsules were attached to polystyrene rods with discs on each end of the rod to center the rod along the centerline of the beam port. The rod was then placed in the inner section of the beam port and the inner beam plug was then pushed in against the rod. The reactor was then brought up to the desired power via square wave, and the foils were irradiated.

Beam ports 3 and 4 are semi-permanently modified at present, and as such, were not available for flux mapping.

The gamma dose in beam port #1 is shown in Figure 13. The gamma dose in beam port #2 is shown in Figure 14. The thermal neutron flux in beam ports 1 and 2 is shown in Figure 15. The change from a "linear" slope (actually an exponential) occurring at the two outer most points may be the result of neutrons scattering off of the inner shield plug, whose inner end was at about 39 inches from the inner end of the beam ports. The cadmium ratio, measured with gold foils, is shown in Figure 16. The relative fast neutron flux for the inner end of beam ports 1 and 2 is listed in Table 1, along with the thermal neutron flux, gamma dose, and cadmium ratio encountered at the inner end of the beam ports.
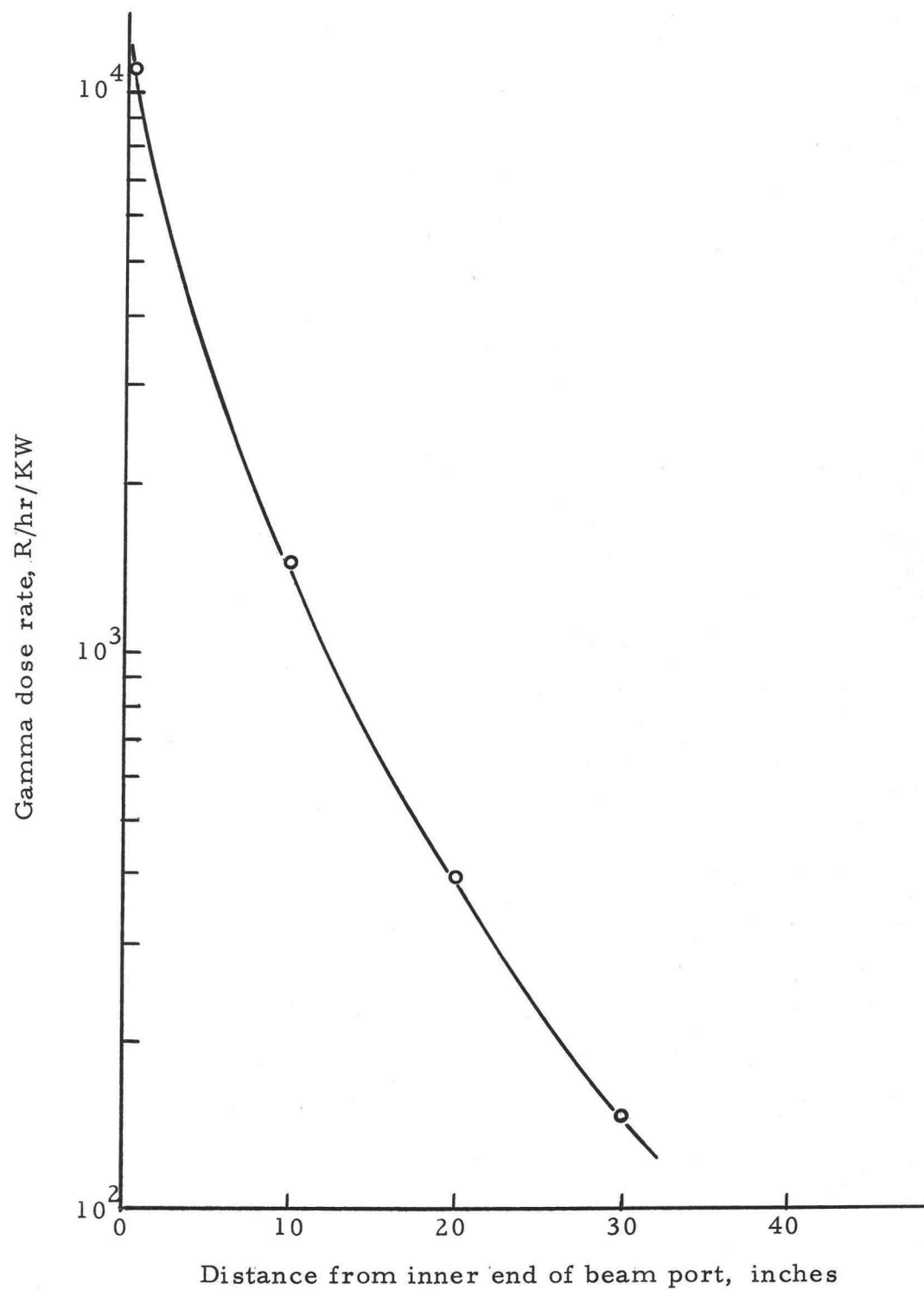
Figure 13.   Gamma dose rate, beam port #1.
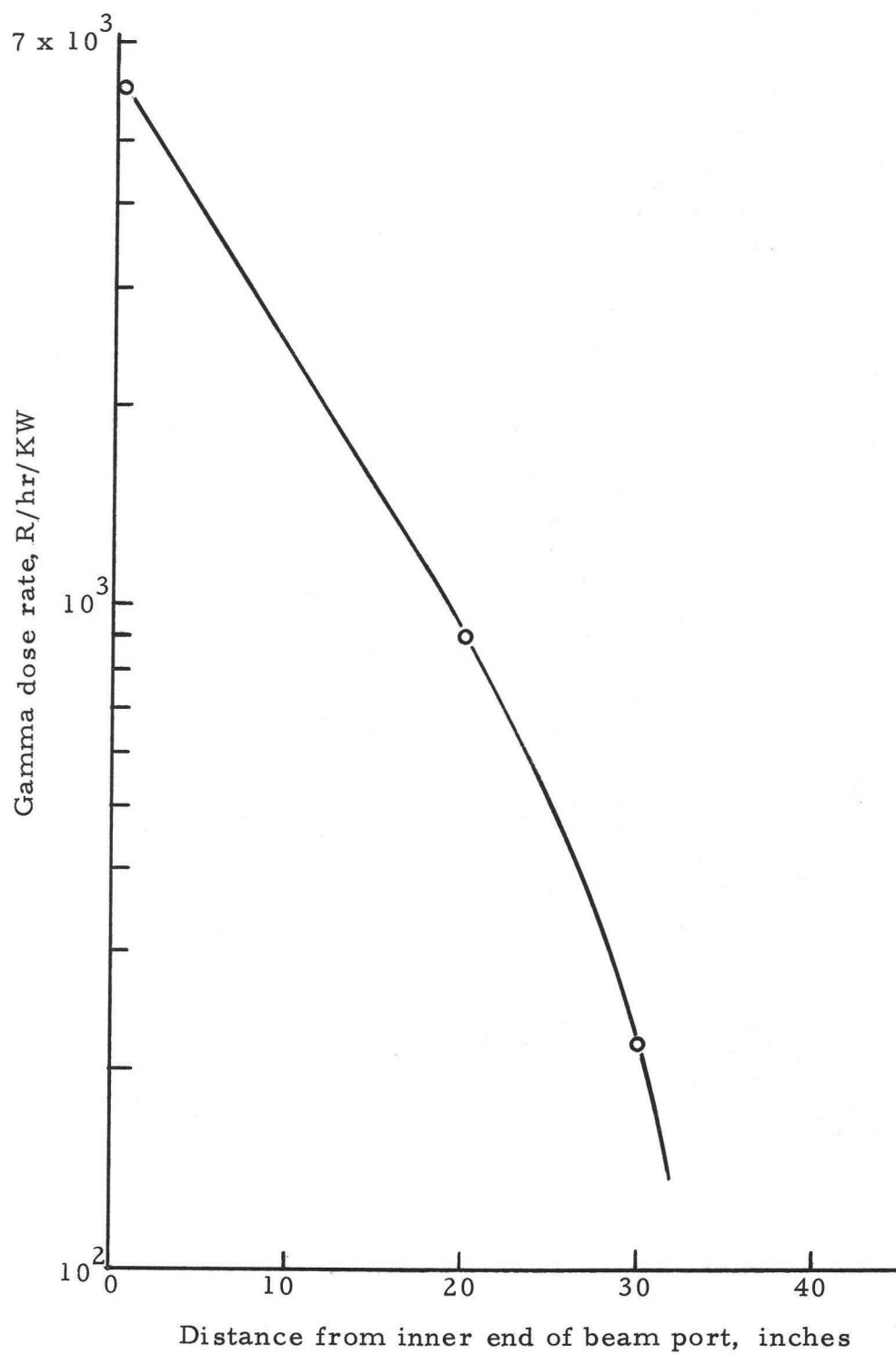
Figure 14.   Gamma dose rate, beam port #2.
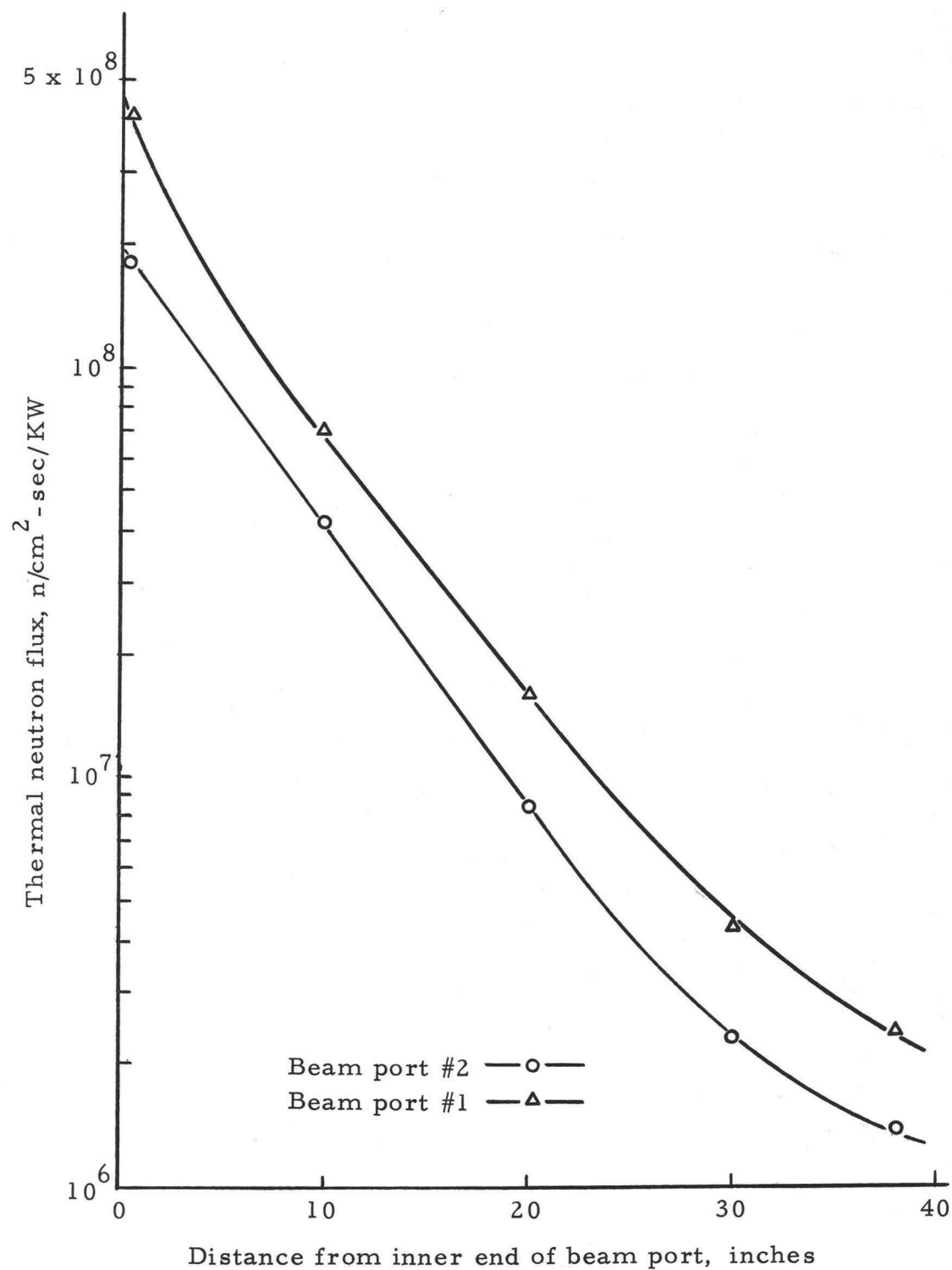
Figure 15. Thermal neutron flux beam port 1 and 2.
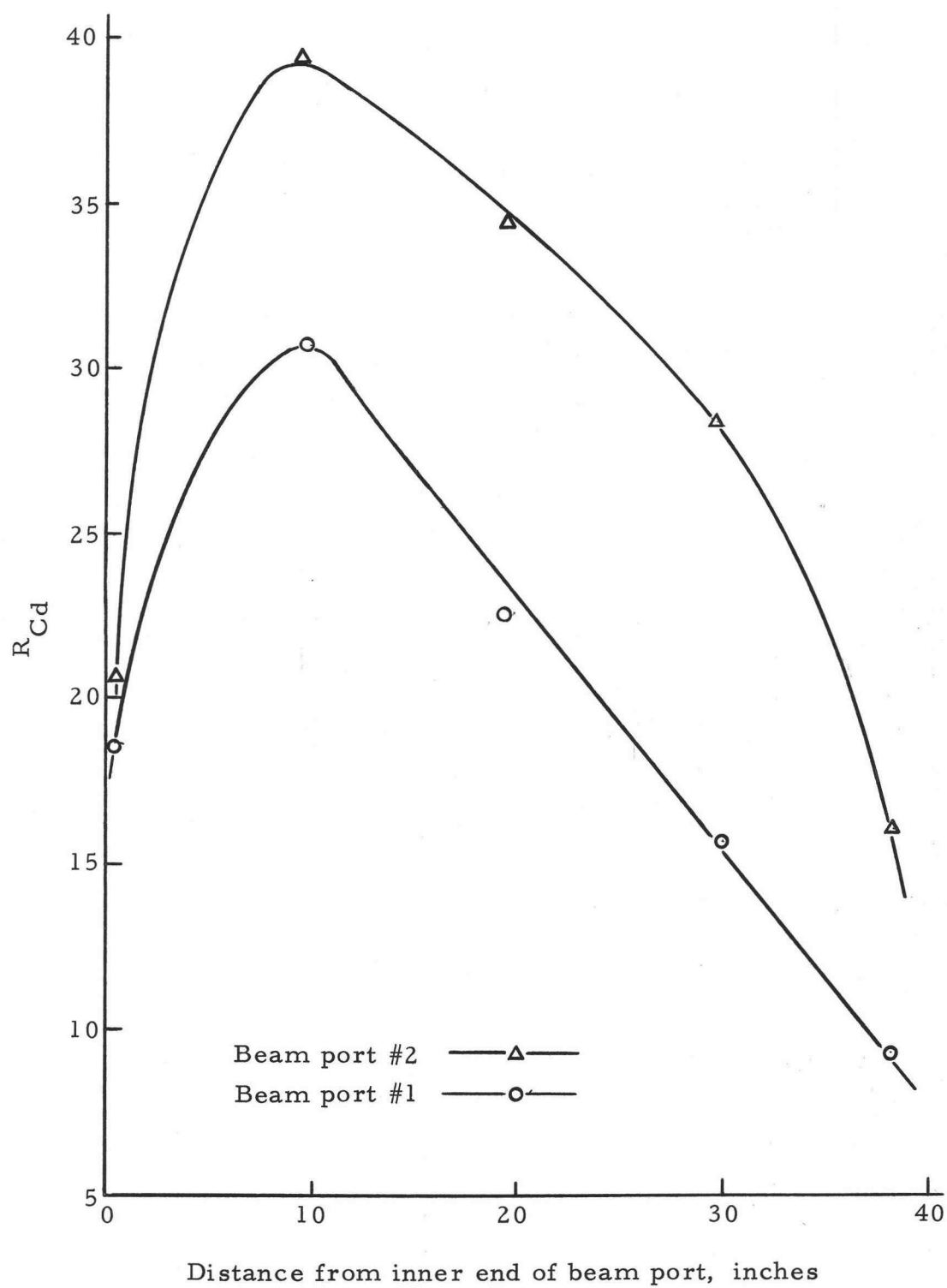
Figure 16.   Cadmium ratio, beam ports 1 and 2.   Measured with solid (10 mil) Au foils.

Thermal Column and Bulk-Shielding Experimental Tank

Thermal Column

The thermal-column is a large, boral lined, graphite-filled aluminum container. Its outside dimensions are four feet by four feet in cross section by approximately five feet three inches in length. The horizontal centerline coincides with that of the active core lattice. In a vertical plane the column extends approximately 13 inches above and below the reflector. The reflector-thermal column relationship is shown in Figure 3. The thermal column is also shown in Figures 1 and 2.

The aluminum container is open toward the reactor room. Blocks of nuclear grade graphite occupy the entire void of the aluminum container. Five graphite blocks serve as removable foil stringers. The central block is aligned with the stringer access plug in the thermal column door. Thus, this central stringer can be removed and inserted without having to move the entire door. To gain access to the other four stringers, the thermal column door must be rolled back on its tracks.

To map the neutron flux, gamma dose, and measure cadmium ratios, foils and LiF capsules were attached to polystyrene rods which were then placed in the voids created by removing the graphite stringers. The graphite thermal column, showing the numbering of

the graphite stringers, is shown in Figure 17.

The thermal neutron flux, measured in four of the stringers, is shown in Figure 18. Cadmium ratios, measured with manganese foils, are plotted in Figure 19. The gamma dose in the central graphite stringer is shown in Figure 20.

Thermalizing Column and Bulk-Shielding Pool

The thermalizing column is similar to the thermal column, but smaller. Its outer section extends from the bulk-shielding experimental tank through the concrete shielding and up to the aluminum reactor tank. The inner section of the column is welded to the tank, and extends to the reflector assembly and matches its contour. The thermalizing column and bulk-shielding pool are shown in Figures 1 and 2. The relation of the thermalizing column to the reflector is shown in Figure 3.

The thermalizing column is two feet by two feet in cross section, by approximately 4 feet 4 inches long. At the inner end (the end nearest the reactor core), the column is filled with graphite blocks to an axial thickness of eight inches. This eight inch wall of graphite is backed by a two inch thick lead slab. Following this is a void approximately 1-1/2 feet long. The outer end of the thermalizing column contains graphite stacked 24 inches thick.

The thermalizing column leads into the bulk-shielding

46.75 in.

46.75 in.

#1

#2

#3

#4

Removable graphite
stringer 4" x 4" x 50" typ.
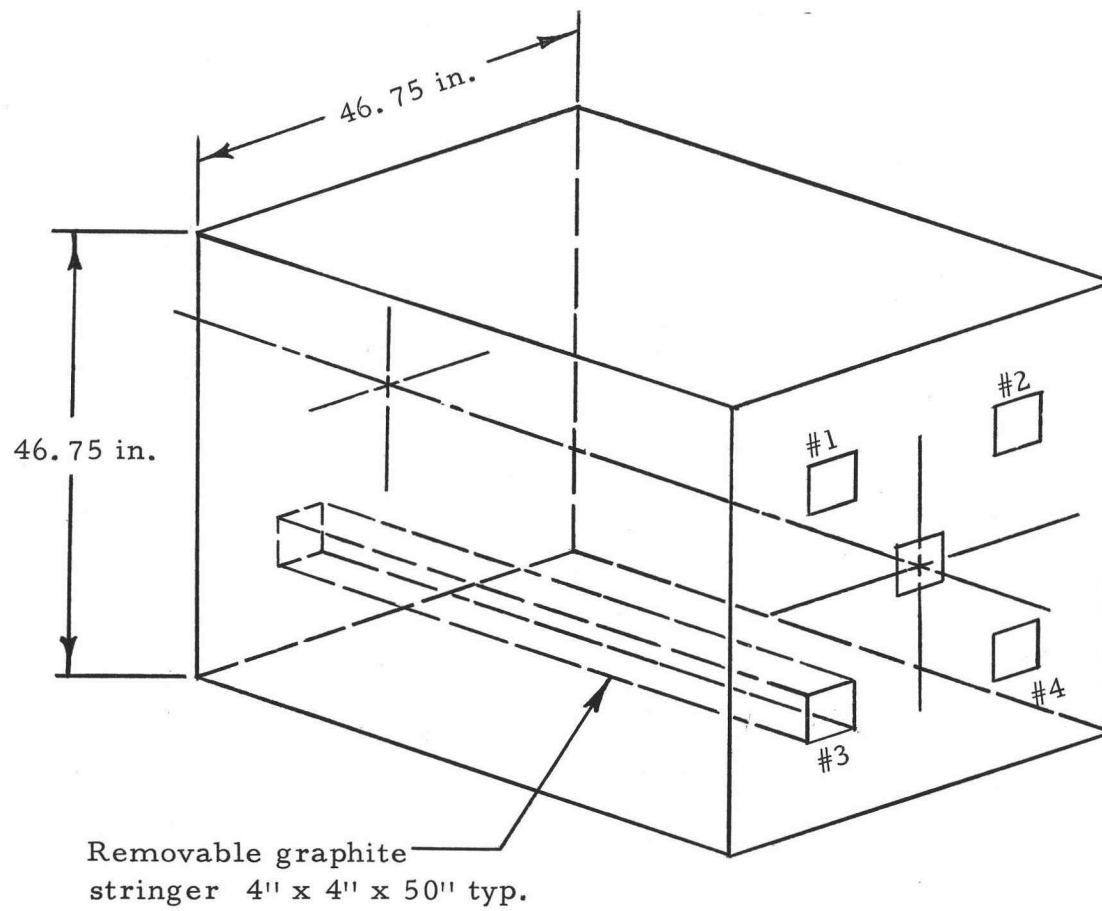
Figure 17.   Graphite thermal column.
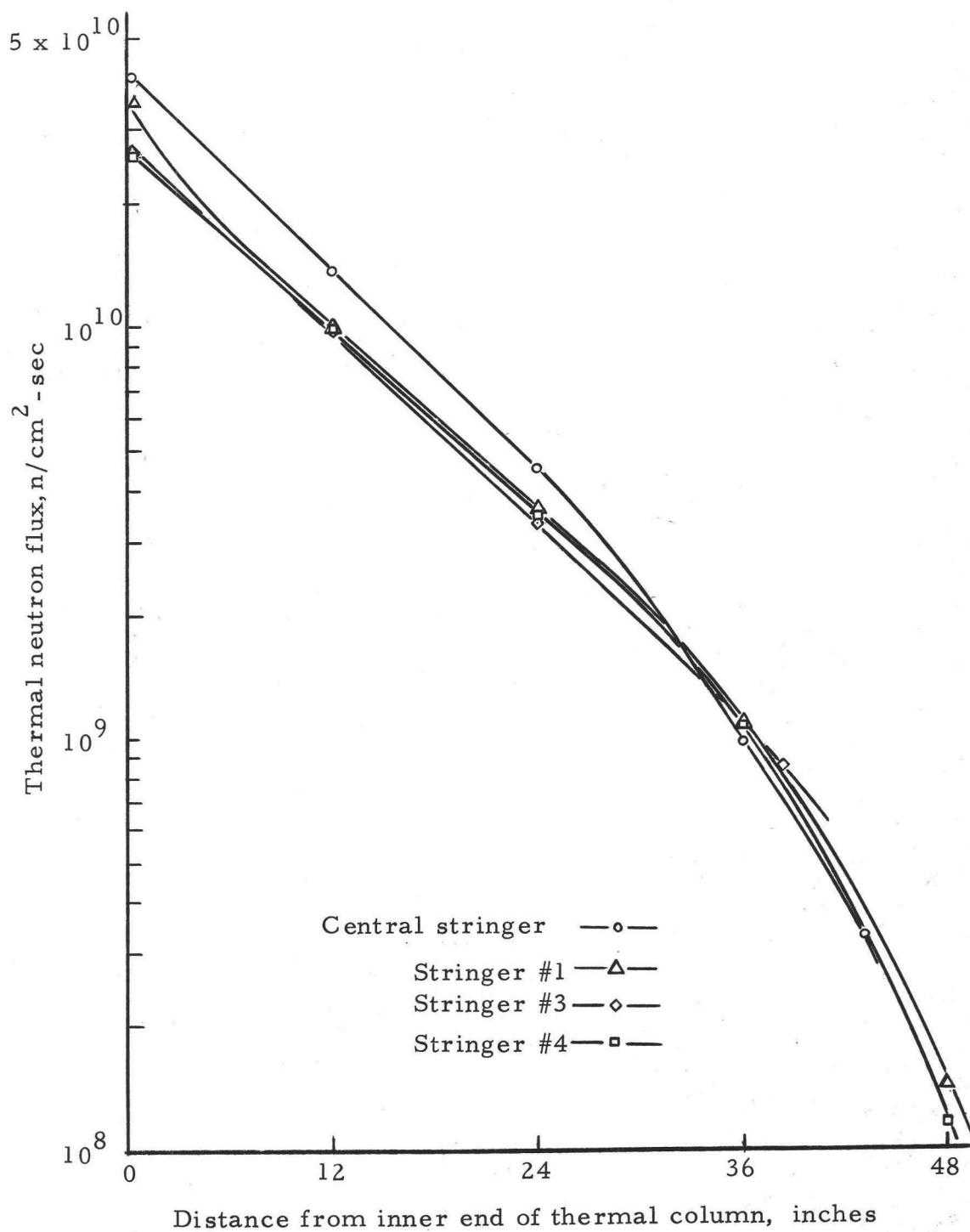
Figure 18.   Thermal column neutron flux, 250 KW.
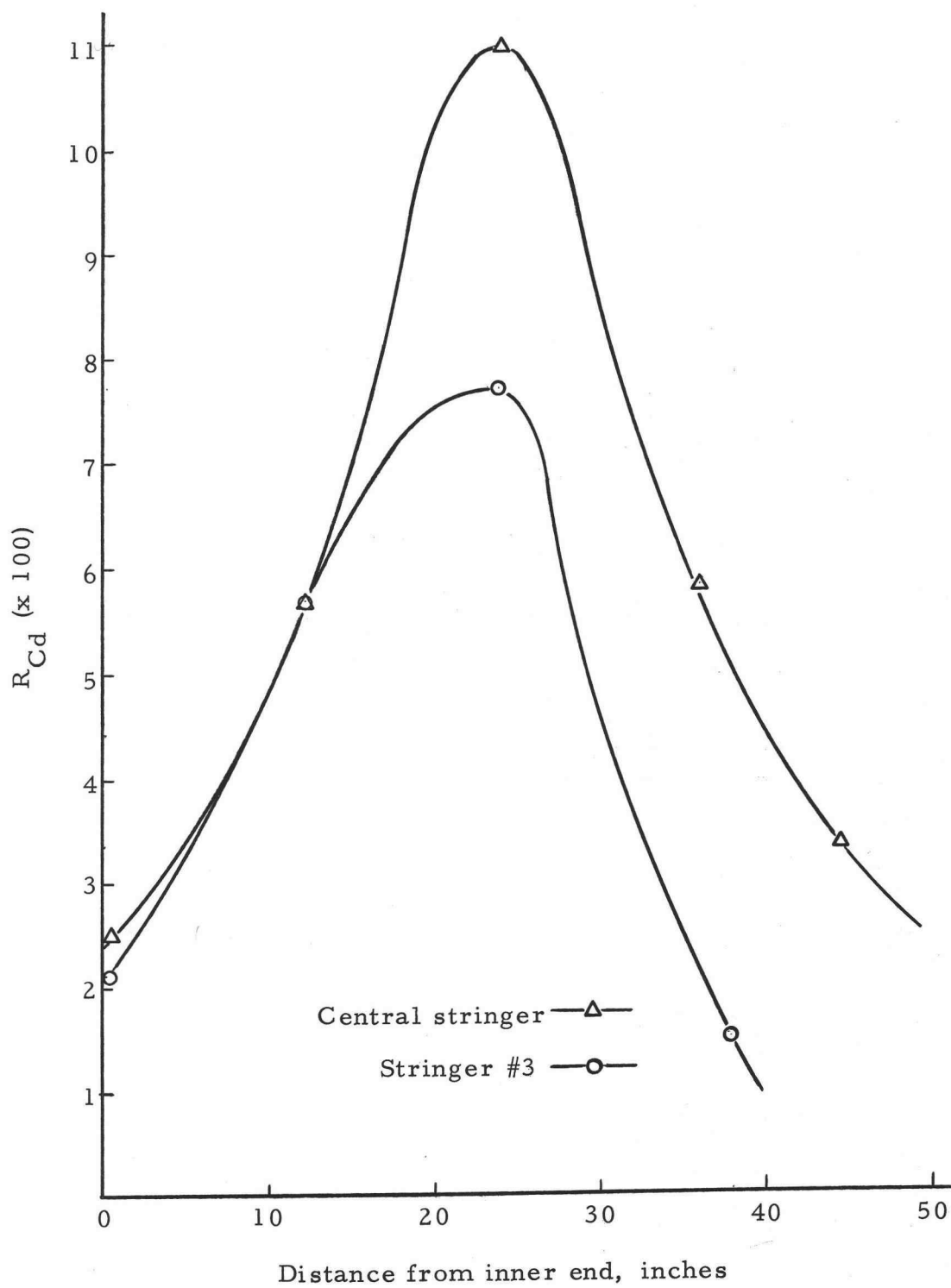
Figure 19. Graphite thermal column, cadmium ratio measured with Mn foils.
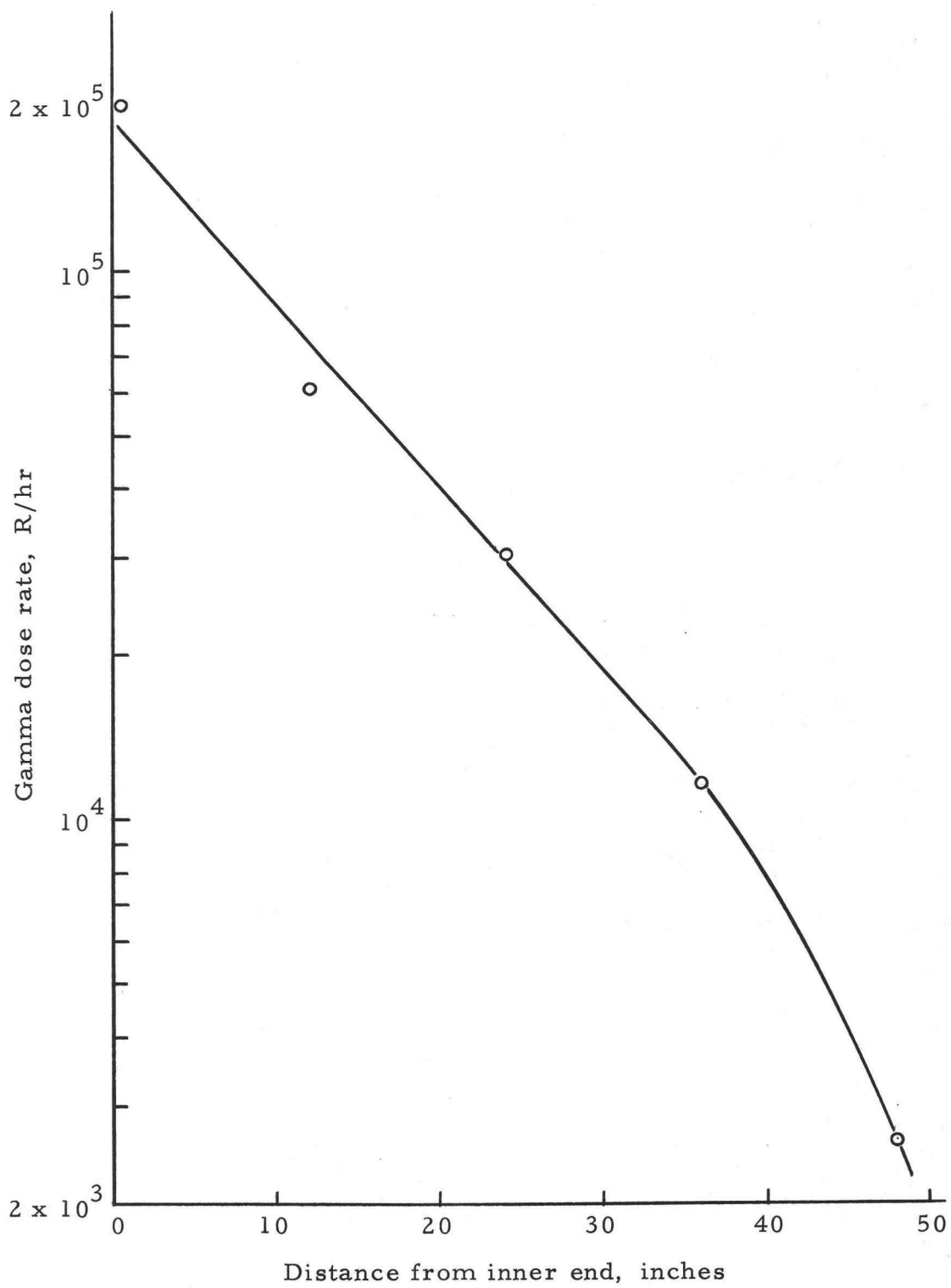
Figure 20. Gamma dose rate, central stringer of thermal column, 250 KW.

experimental tank. The tank is 12 feet deep, eight feet wide, and nine feet long, and is filled with water for shielding purposes.

Thermal neutron flux was measured in three dimensions in the pool. The nomenclature for the flux distribution measurements is shown in Figure 21. The neutron flux was measured along the center-line of the thermalizing column projected into the pool (Y axis), along the vertical centerline of the outer end of the thermalizing column (Z axis), and along the horizontal centerline of the outer end of the thermalizing column (X axis). The thermalizing column is inaccessible for irradiation purposes, hence these flux measurements were taken entirely in the pool facility. The results of the neutron flux measurements are shown in Figure 22. The gamma dose in the pool facility was measured along the Y axis, and the results are shown in Figure 23.
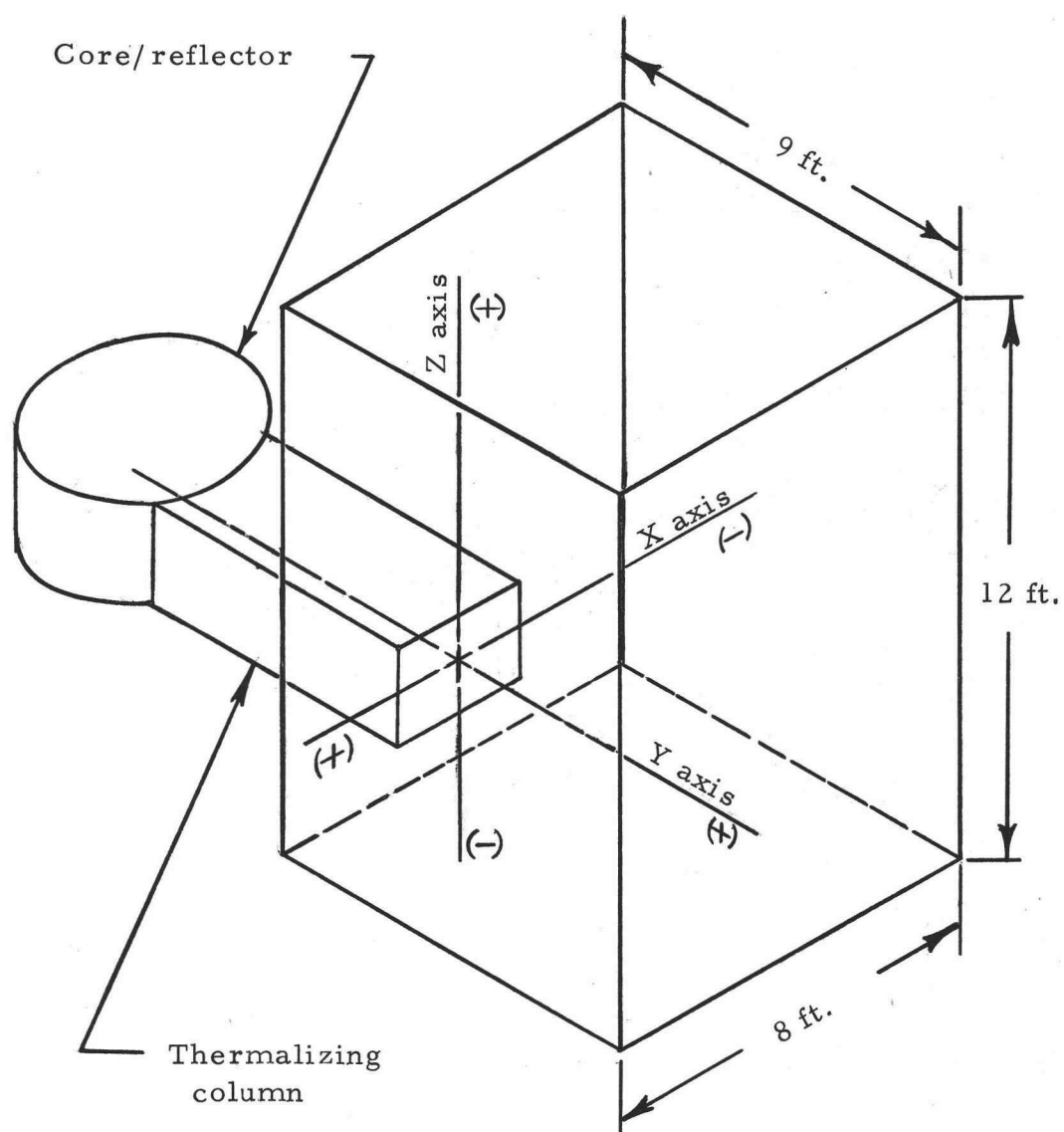
Figure 21. Pool irradiation facility, nomenclature for gamma and neutron measurements.
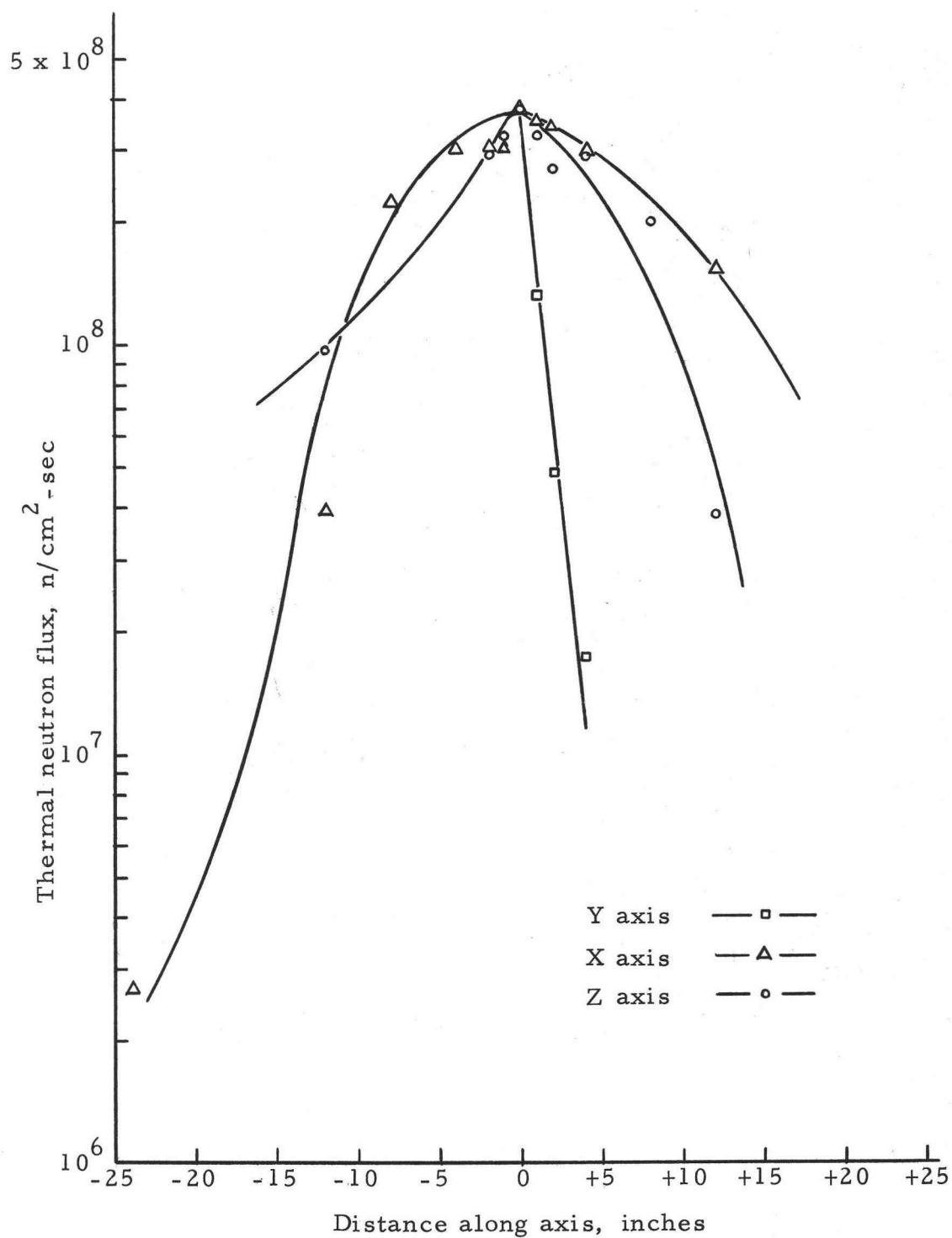
Figure 22. Pool irradiation facility, thermal neutron flux
distribution, 250 KW.
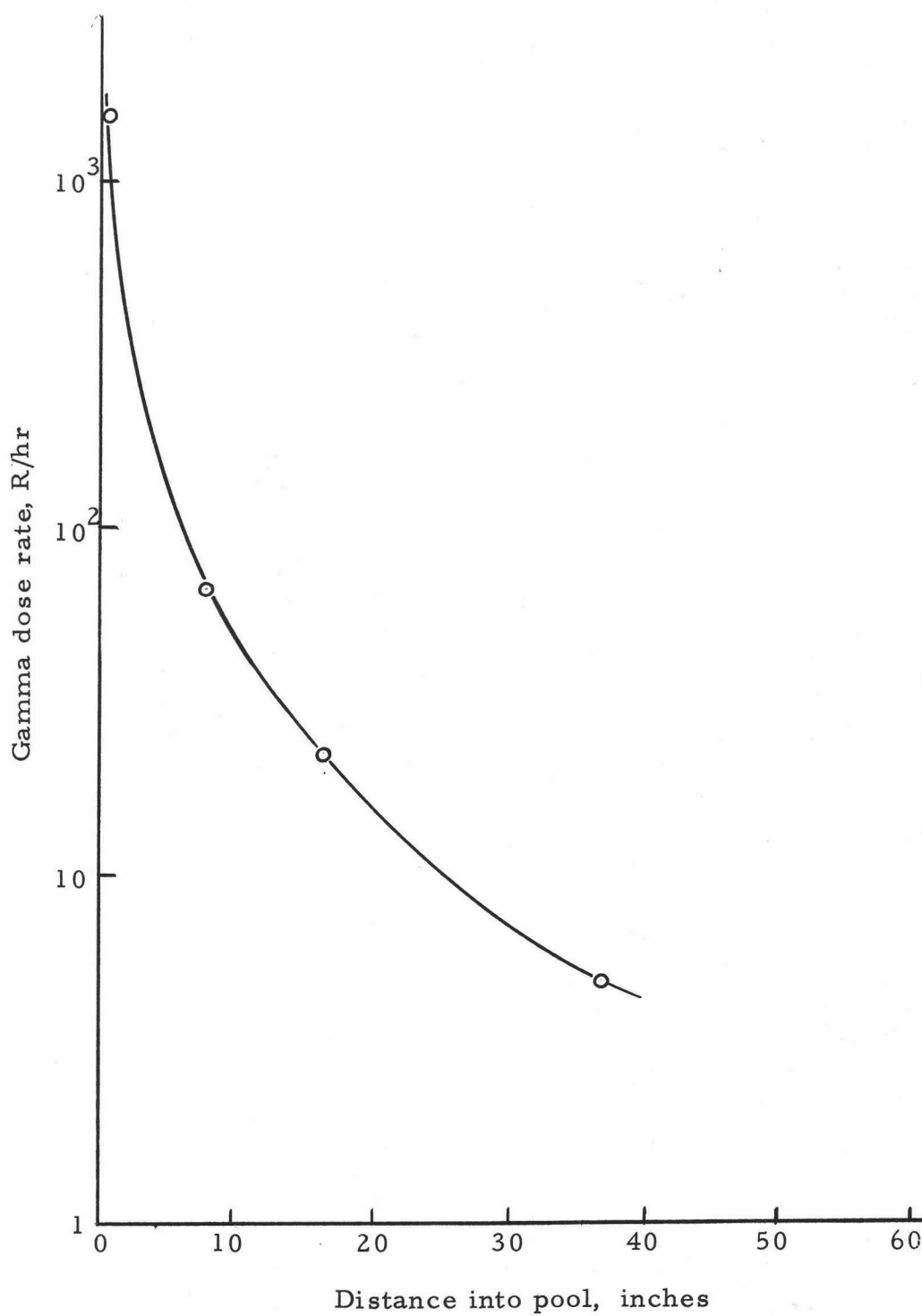
Figure 23.   Gamma dose rate distribution, pool irradiation
facility, 250 KW.

EXPERIMENTAL METHODS

Gamma Dose Measurement

Selection of a Dosimeter

As part of this work, it was desired to measure the gamma
dose in various experimental facilities of the reactor. Requirements
for a gamma dosimetry system included the ability to measure a wide
range of doses, desirability of small size, ability to allow irradiation
without electronic hookups (which might present a problem say in the
rotating specimen rack with the rack rotating), chemical inertness,
ease of use, low cost, and insensitivity to reactor neutrons.

A thermoluminescent dosimetry system was chosen because
of its ability to largely fulfill the above criterion. Lithium fluoride
crystals were chosen for use with the thermoluminescent system be-
cause of the following properties:

1. Wide range of dose measurements, from a few mR up to
    10^5 R.

2. Linearity of response to various energy gamma photons. At
    30 KeV the response is only 25 percent greater than at 1.25
    MeV (3). The energy dependence of LiF dosimeters is giv-
    en in Figure 24.

3. Dose retention. The stored thermoluminescence decays
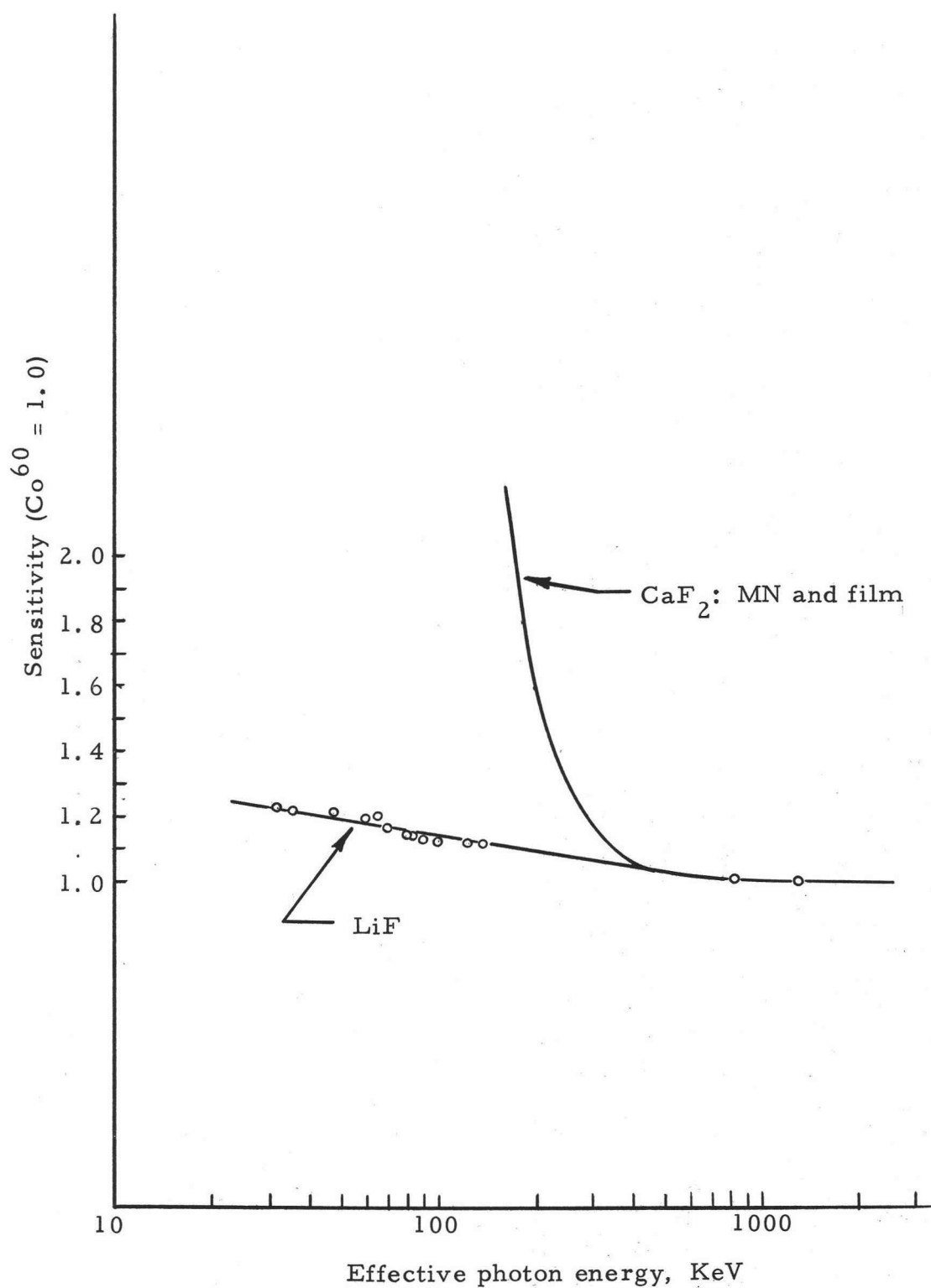
Figure 24. Energy dependence of TLD-100 LiF compared with that of other unshielded dosimeters.

less than five percent per year and is unaffected by visible
light, moisture or mechanical vibration (3).

4. Re-usability. The dosimeters may be annealled and re-
    used if they have not been exposed to excessively high
    doses; at doses on the order of 10^5 R permanent damage is
    encountered. This property of re-usability is attractive
    from a cost standpoint.

5. Negligible dose-rate dependence up to electron beam dose
    rates of at least 2×10^8 Rad/sec, and up to at least 10^{10}
    Rad/sec for x-ray pulses (16).

6. Insensitivity to thermal neutrons. Natural lithium fluoride
    has 7.5 percent Li^6, which has a 945 barn thermal neutron
    cross section. Lithium fluoride consisting of highly en-
    riched Li^7 is commercially available. $Li^7 F$ retains the
    identical gamma-measuring properties of $Li^6 F$, and the
    removal of Li^6 makes the $Li^7 F$ material relatively insen-
    sitive to neutrons (21).

7. The powder form in which the LiF crystals are supplied
    makes for a very versatile dosimeter.

Theory of Thermoluminescence

The exact mechanism of thermoluminescence is not perfectly
understood, but the current theoretical interpretation is as follows

(15): impurity atoms or other crystal lattice defects provide meta-
stable electron states several eV above the ground state. When the
crystal is exposed to ionizing radiation, electrons are freed from the
ground state and they may become trapped in the metastable electron
states. When the crystal is heated to the required temperature, ther-
mal excitation energy dislodges electrons from the traps. They re-
turn to the ground state, radiating light in the visible and near-visible
spectrum. The electron traps have been found to fall into several
groups, each with a characteristic temperature at which the electrons
are released. The temperatures of release are characteristic of the
type of crystal and the impurities.

The phenomenon of thermoluminescence is used to measure
radiation dose by exposing a quantity of powder to the dose to be
measured. The number of electrons that become excited and trapped
is proportional to the amount of absorbed radiation. The exposed
sample is then heated, and the amount of light given off is measured,
giving a reading proportional to the radiation dose.

Mechanics of Thermoluminescent Dosimetry

Two types of thermoluminescent material were utilized in this
work. They were natural lithium fluoride and lithium fluoride en-
riched to 99.993% Li[7]. Both were supplied by Controls for Radiation,
Cambridge, Massachusetts. The commercial designation for natural

lithium fluoride is LiF-N, and for enriched Li^7 it is LiF-7, this nomenclature will be used henceforth. The LiF powders were supplied in three gram lot sizes, the grain size is 80-200 mesh.

The LiF powder was dispensed into small cylindrical (3/4 inch x 1/8 inch. I.D.) polyethylene capsules. The dispenser was a vibrator compactor. The vibrator dispensed on the average a 39.11 milligram sample with a standard deviation of 0.018 milligrams, or a standard error of 0.34 percent.

LiF samples that had been exposed to a radiation dose were read with a thermoluminescent reader. The instrument used was a Madison Research Model S-2LC TL Reader. The instrument consists of two basic operational systems, both controlled by a single sequential timer. One of these systems heats the luminescent material in a controlled manner to release the radiation-induced luminescence while the other system measures the amount of luminescence given off by the heated sample. The sample is heated by a high amperage current in a silver pan to reduce black body radiation. The light output of the heated sample is read by a photomultiplier tube. The anode current from the photomultiplier tube is directly proportional to the thermoluminescence released from the sample. The anode current is integrated over the total reading cycle to determine the total thermoluminescence emitted. This is accomplished by using a simple analog-digital converter and summing the digits with

decade counters.

The digital counter is just one of two ways that the thermoluminescent output can be recorded. The photomultiplier tube current can be read from output terminals located on the TL reader. A Keithley electrometer/Moseley strip chart recorder, Fluke Galvanometer/recorder, or equivalent combination may be connected to monitor photomultiplier tube current. The recording of the photomultiplier tube current as a function of time gives a characteristic "glow curve."

Glow curves are useful in many investigations and in adjusting the instrument parameters of the TL reader. Counts or glow curves may be recorded individually or simultaneously.

Glow curves for various doses from Co^{60} irradiation of LiF-N dosimeters were recorded with a Fluke galvanometer/Honeywell 2106 visicorder. These glow curves are shown in Figure 25. These curves are shown for illustrative purposes only, as the digital readout was used exclusively in dose determination work.

Calibration of the Thermoluminescent Reader

The calibration curve for LiF powder used in conjunction with the thermoluminescent reader is shown in Figure 26. The LiF powder samples, both LiF-7 and LiF-N, were irradiated in a cobalt-60 irradiator. The present source strength of the Co^{60} irradiator is
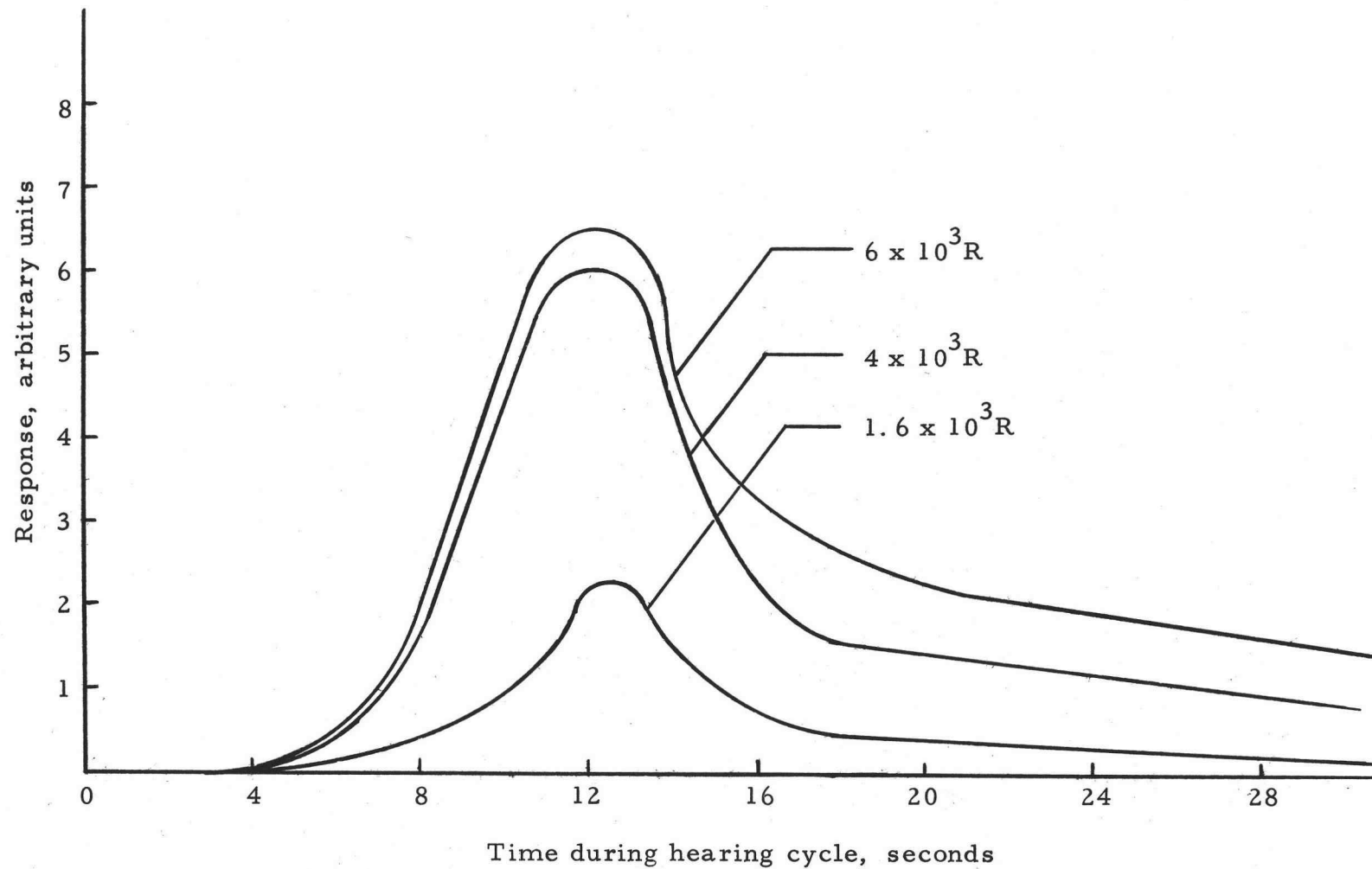
Figure 25. Glow curves obtained from readout of LiF samples exposed to various doses of Co^{60} radiation.
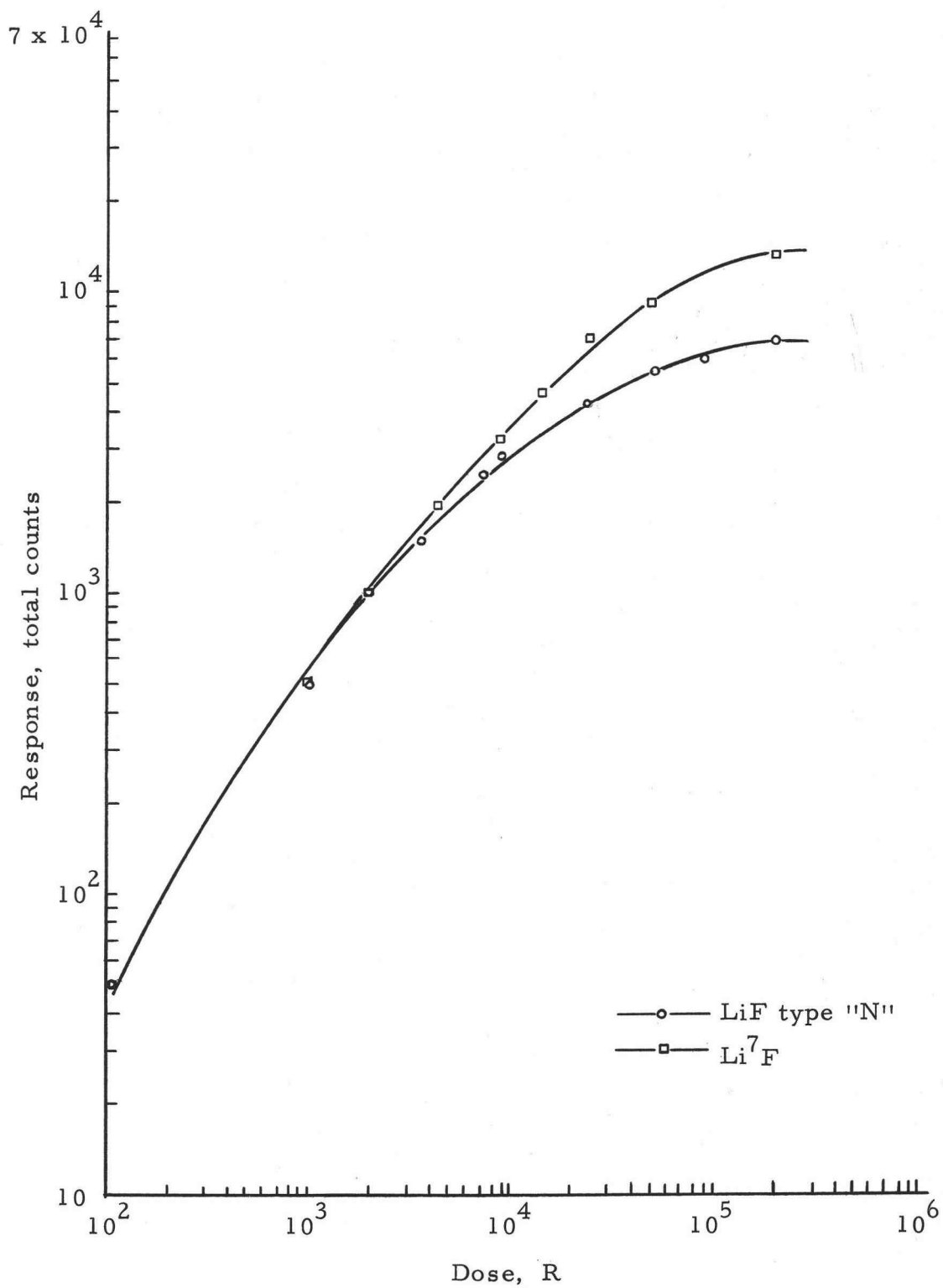
Figure 26.   Thermoluminescent response of Lithium Fluoride to Co^{60} gamma irradiation.

approximately 1800 curies. Maximum dose rates obtainable are on

the order of 5.6 x 10^5 R/hr. The LiF samples having been exposed

to varying doses of radiation were then read on the thermolumines-

cent reader. Hence a graph of reader response vs. dose was obtained

for the LiF powder. For doses in the range 10 R to 100, 000 R the

manufacturer recommends a TL reader photomultiplier voltage of

750 V and a gain of two. These values were used throughout this

work.

Considerations in the Use of LiF for Gamma Dose Determination in a Reactor Environment

It became apparent early in this work that the LiF type N would

be unsatisfactory for gamma dose work in the reactor. The large

thermal neutron cross section of Li^6 that is present in LiF type N

makes the LiF-N sensitive to thermal neutrons. The Li^6 absorbs a

thermal neutron and emits an alpha particle thusly: $Li^6(n, a)H^3$. The

total energy of the recoil particles is 4.8-MeV, a 2.05-MeV alpha and

2.75 MeV H^3. The recoiling particles cause thermoluminescent ef-

fects in the LiF-N crystals. Thermoluminescence effects of alpha

particles in LiF is detailed in Reference 15.

It was believed that LiF-7, reported by the supplier to be

99.993 percent enriched in Li^7, would be relatively insensitive to

thermal neutron exposure. Such was not the case. Both LiF-7

and LiF-N were irradiated bare and cadmium covered simultaneously in the reactor. Since the cadmium covers effectively shielded out all of the thermal neutrons it was not surprising that the cadmium-covered LiF-N and cadmium-covered LiF-7 registered essentially the same TL response. The surprising result was that the TL response of the bare LiF-7 was essentially the same as the TL response of the bare LiF-N. The response of the bare LiF powders were approximately 1.75 times that of the cadmium covered LiF powder. The LiF-7 obviously was sensitive to thermal neutrons. This has been reported by other investigators (6). Within the high thermal-flux environment of reactors the response of LiF-7 to thermal neutrons is approximately 65% of the total response of the phosphor to the mixed (γ + neutron) radiation field (6). Because of the large thermal-neutron cross section, even trace amounts of Li^6 present in the LiF-7 will significantly bias the gamma dose results in exposure environments containing high fluences of thermal neutrons (6). That this is primarily due to the thermal neutron response of the LiF-7 has been verified by Wingate et al. (6). All gamma work in the reactor thus utilized small closed cadmium cylinders surrounding the LiF samples. Cadmium does have a high (n, γ) cross section for thermal neutrons. However, the gamma fluence resulting from neutron capture in the cadmium cylinders was calculated to be insignificant in comparison to the gamma flux being measured. Cadmium was used

for the neutron shield because of its availability, and ease of fabrication. The cadmium shields did not attenuate the gamma flux. This was determined by using the Co^{60} irradiator to expose shielded and unshielded LiF samples to identical gamma doses. The response of the shielded and unshielded dosimeters was identical.

The TL response of LiF to fast neutrons has also been investigated (10, 11). Kastner et al. (10) report that exposure of ^{7}LiF powder to fast neutrons in the range 100 to 1000 KeV affects the TL response of Li^{7}F to gamma rays. One group of dosimeters were given an exposure to Co^{60} gamma rays of 3.1 R and a subsequent irradiation with neutrons of 0.1, 0.26, and 1.0 MeV. Another group of dosimeters were irradiated simultaneously with Co^{60} and fast neutrons of the above energy grouping. The percentage drop in thermoluminescent response was approximately constant regardless of whether the neutron exposure is carried out simultaneously with or following the gamma irradiation. The percentage drop in response is also independent of neutron energy and total exposure. The drop in the thermoluminescent response of the ^{7}LiF was approximately ten percent.

The results reported by Kastner are not comprehensive enough to predict the effects of fast neutron exposure on the gamma response of Li^{7}F dosimeters in general. The gamma doses measured in this work were on the order of 10^3 to 10^4 R. These doses are several

orders of magnitude greater than the dose used in Kastner's study.
Thus it is extremely difficult to say that fast neutron exposure simul-
taneous with gamma exposure will cause a ten percent decrease in
gamma response (as reported by Kastner) for gamma doses in the
range 10^3 to 10^4 R.

Wingate et al. (7) have reported a fast neutron response for
LiF-7 equivalent to approximately $0.2R/(10^{10} n/cm^2)$ for neutron
energies of 0.3 to 1.3 MeV. Since all in-core LiF irradiations were
made at low power levels the neutron flux in the above energy range
is not great enough to make a significant contribution to the response
of the LiF-7 dosimeters.

Discussion of Errors

The standard error associated with the gamma dose measure-
ments was in the range 1-1/2 to 5 percent. The standard error gen-
erally was highest for low doses, and decreased with increasing dose.

The error associated with the Co^{60} dose used to calibrate the
TL reader is on the order of ten percent (17).

Thus the total experimental error associated with a given gam-
ma dose measurement is in the range 12 to 15 percent.

Thermal Neutron Flux Measurement

Neutron Flux, Reaction Rate, and Cross Section

The generalized definition of neutron flux is

$$\phi = \int n(v)v\,dv = n\bar{v} \tag{1}$$

in which $n(v)dv$ represents the number of neutrons per unit volume having speeds within an interval dv about v, n is the total neutron density, and $\bar{v}$ is the average neutron velocity.

A more important concept is that of reaction rate, which also involves the cross section for neutron interaction, σ. The cross section is a statement of the probability that the reaction will take place. In general, cross sections are velocity (or energy) dependent. Thus it is necessary to keep the factors $\sigma(v)$, $n(v)$ and v together in each velocity interval when carrying out an integration over all neutron energies. Thus, the reaction rate per target nucleus is given by

$$r = \frac{R}{N} = \int \sigma(v)n(v)v\,dv \tag{2}$$

Equation (2) can also be expressed as

$$r = \frac{\int \sigma(v)n(v)vdv}{\int n(v)vdv} \times \int n(v)vdv \tag{3}$$

The first factor is recognized as an average cross section, namely that averaged over the neutron flux spectrum

$$\overline{\sigma} = \frac{\int \sigma(v)n(v)vdv}{\int n(v)vdv} \tag{4}$$

so that

$$r = \overline{\sigma}\phi \tag{5}$$

Using Equation (1), Equation (5) may also be written $r = \overline{\sigma}n\overline{v}$. It must be remembered however that $\overline{v}$ is averaged over the neutron density spectrum, $n(v)$, whereas $\overline{\sigma}$ is averaged over the neutron flux spectrum, $n(v)v$.

For flux to have meaning it must be accompanied by other information that characterizes adequately both $n(v)$, the neutron spectrum in the reactor, and $\sigma(v)$, the cross section dependence of the nuclide whose reactions are of interest. Hence the term flux is frequently modified by an adjective that refers to a specific section of the neutron energy spectrum, i. e. slow or thermal neutron flux.

"Thermal neutron flux" is most frequently quoted, as most

reactors in existence today are "thermal." In a thermal reactor the neutrons are born with energies in the MeV range (velocities on the order of 10^9 cm/sec). These neutrons make a large number of collisions with nonabsorbing nuclei (the moderator) before they are ready to be captured. In the early collisions a neutron loses most of its kinetic energy. It is left with "thermal" values of this energy, near 1/40 eV (velocities on the order of 10^5 cm/sec). In the subsequent collisions, it sometimes loses and sometimes gains kinetic energy from the thermally agitated nuclei of the lattice. The time spent in the thermal region is generally long compared to the slowing-down time. If one could take a picture of all neutrons present in the reactor, and if each neutron was labeled by its instantaneous velocity, it would be possible to deduce from this photograph the function $n(v)$, the neutron spectrum. If this were plotted against v, a curve would result that has a shape similar to the Maxwellian distribution of the molecular speeds in a gas

$$n(v) = \frac{4n}{\sqrt{\pi}} \frac{v^2}{v_0^3} \exp \left(\frac{-v^2}{v_0^2} \right) \tag{6}$$

Where n is the total number of neutrons per cm^3, and v_0 is the most probable neutron velocity, or the velocity at which this distribution assumes its maximum. It is related to the absolute

temperature, characteristic of the equilibrium, by

$$\frac{mv_0^2}{2} = kT \tag{7}$$

where

m = mass of neutron (1.67×10^{-24} gram)

k = Boltzmann constant 1.38×10^{-16} erg deg^{-1}

T = temperature (^{O}Kelvin)

At room temperatures $T = 293$ and $V_0 = 2200$ m/sec.

This velocity v_0 is not the average velocity in the Maxwellian distribution. The average velocity is found by multiplying the Maxwellian distribution (Equation (6)) by v and integrating over all velocities:

$$\overline{v}_M = \frac{\displaystyle\int_0^\infty vn(v)dv}{\displaystyle\int_0^\infty n(v)dv} = \frac{4}{\sqrt{\pi}} \int_0^\infty e^{-(\frac{v}{v_0})^2} (\frac{v}{v_0})^3 dv = \frac{2}{\sqrt{\pi}} v_0 \tag{8}$$

which shows that the average velocity is greater than the most probable velocity by a factor of $2/\sqrt{\pi}$, or 1.128. According to Equation (1) the Maxwellian thermal flux is given by:

$$\phi_M = n\overline{v}_M$$

When this definition of thermal flux is used, the cross section averaged over the Maxwellian flux spectrum, calculated according to Equation (4), is the only legitimate cross section by which to multiply ϕ_M to get a reaction rate.

Capture cross sections of many elements (such as gold and manganese) are proportional to $1/v$ in the thermal range of neutron energies. The "straight line" portion of the total cross section of gold, shown in Figure 27, is the $1/v$ region of gold cross section. The function $\sigma(v)$ becomes a constant divided by the velocity

$$\sigma(v) = \frac{\sigma_0 v_0}{v} \tag{9}$$

In most tabulations of thermal capture cross sections, e.g. BNL-325(9), the cross sections quoted are values of σ_0 corresponding to the velocity $v_0 = 2200$ m/sec (the most probable Maxwellian velocity at $T = 293\,^{\circ}K$). For a $1/v$ velocity dependence, the average capture cross section in any flux spectrum is found by substituting (9) into (4) and using (1) for ϕ:

$$\bar{\sigma} = \frac{\int (\frac{\sigma_0 v_0}{v}) n(v) v\, dv}{\int n(v) v\, dv} = \frac{\sigma_0 v_0 n}{\phi} = \frac{\sigma_0 v_0}{\bar{v}} \tag{10}$$

In the case of a Maxwellian shape of $n(v)$ and a $1/v$
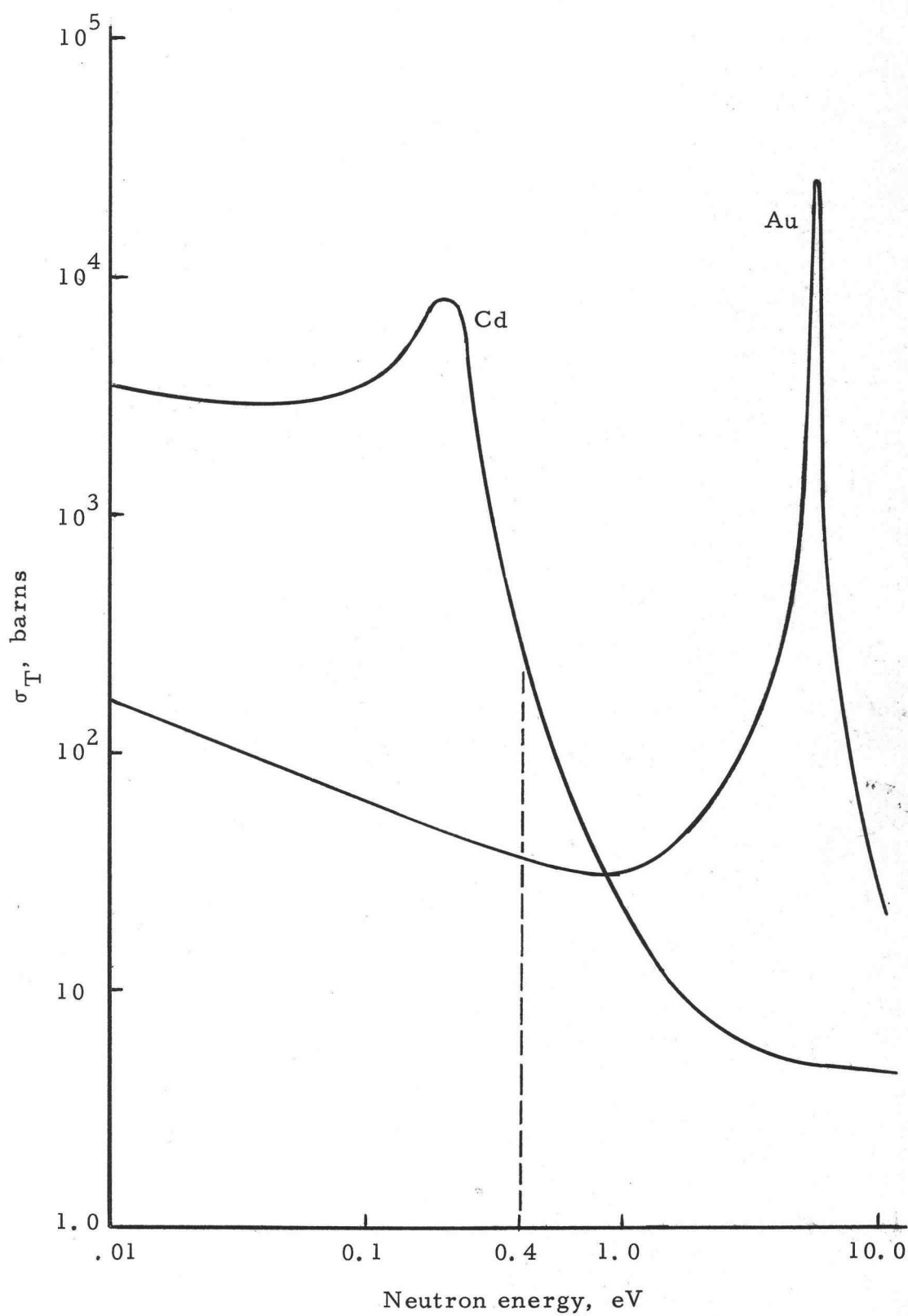
Figure 27. Total cross section of cadmium and gold at various energies.

dependence of σ and using Equation (8) we see that

$$\overline{\sigma}_M = \frac{\sigma_0 v_0}{1.128 v_0} = 0.886 \sigma_0 \qquad (11)$$

Hence the average Maxwellian cross section is not equal to the tabulated thermal cross section, σ_0. The tabulated cross section must be multiplied by 0.886 to arrive at a value that is consistent with the quoted value of the Maxwellian flux, ϕ_M.

Another definition of thermal flux that is frequently used is due to Westcott (25, p. 5) ; instead of multiplying the number of neutrons per unit volume by the average neutron velocity $\overline{v}$, Westcott multiplies the true n by the fixed velocity $v_0 = 2200$ m/sec. for which the cross sections are tabulated, thus

$$\phi_W = n v_0 \qquad (12)$$

regardless of whether or not the neutrons are at room temperature, T_0. The flux concept is essentially replaced by that of neutron density. The corresponding Westcott cross section is given by

$$\sigma_W = \frac{\int \sigma(v) n(v) v \, dv}{n v_0} \qquad (13)$$

For strict $1/v$ dependence of the cross section, we see that by

using Equation (9) that σ_W is exactly equal to the tabulated σ_0, regardless of the neutron temperature or of any other features of the neutron spectrum. Deviations from the $1/v$ dependence are taken care of by correction factors

$$\sigma_W = \sigma_0(g+rs) \tag{14}$$

in which g and s represent deviations from the $1/v$ dependence of the cross section in the thermal and epithermal regions, respectively, and r accounts for the deviation of the spectrum from the Maxwellian shape at the higher energies possessed by fission neutrons and neutrons being slowed down. The convenience of Westcott's method derives from the facts that tabulated values may be used, and that corrections can be easily evaluated from foil activations made inside the reactor (r) and from calculations based on detailed cross section information (g and s). Results of these calculations for some of the more important nuclides are tabulated by Westcott (26, p. 10-24).

To estimate activation rates of specimens to be placed in a given thermal reactor, it is necessary to ascertain what definition was used when the flux level was quoted, and it is necessary to multiply this flux by the appropriate value of the cross section. If the Maxwellian flux is quoted, the tabulated cross section must be reduced by

the factor 0. 886; if the Westcott flux is quoted. The tabulated cross section may be used as is.

Considering that both gold and manganese are essentially 1/v absorbers below the cadmium cut-off (that is, the Westcott g factors are 1. 00) the 2200 m/sec cross section values were used for these materials in all computations of thermal neutron flux. Thus the neutron flux specified is the Westcott flux.

Thermal Neutron Flux Measurement by Foil Activation, Introduction

A common method for determining neutron flux in a given medium is based on counting the beta or gamma-ray activity induced by the neutrons in a foil of suitable material. Desirable qualities of a neutron detecting material include the following:

1. The material should be easily available in a convenient form.

2. The absorption cross section in the energy range of interest should be high.

3. The half life of the resulting activity should neither be so short that most of the activity disappears prior to counting nor so long that the foil cannot be activated to saturation, if required, in a reasonable length of time.

4. The residual nucleus should have a relatively simple decay scheme.

Indium, gold and manganese are materials that meet these criteria well and are in wide use in the measurement of low-energy neutron fluxes.

Of the above three foils, only gold and manganese were used for absolute thermal neutron flux measurements. Indium was used once for a relative thermal neutron flux measurement.

The thermal neutron flux in a medium is determined by exposing bare foils and cadmium-covered foils at the same location and calculating the flux from the difference of the activities produced. This cadmium difference must be corrected for various effects which tend to give a false reading. These effects include the depression of the flux due to the presence of a strong, localized absorber in the neutron field; the self-shielding in the foil, whereby the flux is depressed within the detector resulting in the activation at points within the foil being lower than at its surface; the self absorption in the foil of the radiation emitted by the activated nuclei; absorption of neutrons with energies above the cadmium cut-off by the cadmium covers; and the thermal neutron contribution to the activation of cadmium-covered foils.

Corrections Applied to Foil Measurements and Neutron Flux

Cadmium-covered and bare foils are commonly used in neutron flux measuring experiments to determine the flux above the cadmium

cut-off point which is located at approximately 0.4 eV. An ideal neutron filter would pass all neutrons above a certain energy, and block out all neutrons below that same energy. While no such material exists, cadmium closely approximates this behavior. Cadmium has a high absorption cross section for neutrons below 0.4 eV, and a comparatively low cross section for neutrons above 0.4 eV.

The total cross sections of gold and cadmium as a function of neutron energy are shown in Figure 27. The cross section values were taken from BNL-325 (9, p. 217-296). Since the scattering cross section of cadmium and gold is low and essentially constant with energy, the curves in Figure 27 represent essentially the absorption cross-sections of gold and cadmium, and they show that cadmium effectively acts as a neutron filter.

The cadmium ratio (R_{Cd}) is defined as the saturated activity per gram of a bare foil (A_g^B), such as gold, divided by the saturated activity per gram of the same type of foil completely covered with cadmium (A_g^C)

$$R_{Cd} = \frac{A_g^B}{A_g^C} \tag{15}$$

The cadmium-covered foil responds largely to the flux in its reasonance region.

The cadmium ratio is a measure of how well the neutrons are thermalized.

The cadmium difference is defined as the saturated activity per gram of a bare foil minus the saturated activity per gram of a cadmium-covered foil exposed to the same flux:

$$\text{C. D.} = A_g^B - A_g^C \tag{17}$$

This difference represents the activity produced by neutrons whose energies are less than the cadmium cutoff energy (essentially thermal neutrons).

Two corrections to be considered with the use of cadmium-covered foils are the attenuation of epicadmium neutrons by cadmium covers and the leakage of thermal (or sub-cadmium) nuetrons through the cadmium covers. These two factors are now considered.

The following quantities are first defined:

$(A_g^B)^T$ = total measured bare foil activity.

$(A_g^C)^T$ = total measured cadmium-covered foil activity.

$(A_g^B)^{\text{epi-Cd}}$ = activity of bare foil due to epicadmium neutrons.

$(A_g^B)^{\text{th}}$ = thermal neutron activation of a bare foil.

$(A_g^C)^{\text{th}}$ = thermal component of the cadmium-covered foil activity.

F_{Cd} = correction for absorption of epicadmium neutrons by cadmium.

Using F_{Cd} we can say:

$$(A_g^B)^{epi-Cd} = (A_g^C)^T F_{Cd} \qquad (18)$$

To obtain the true epicadmium activity, the thermal neutron activation of cadmium-covered foils should be subtracted from the total cadmium-covered activity, $(A_g^C)^T$, before the correction factor, F_{Cd}, is applied, thusly:

$$(A_g^B)^{epi-Cd} = ((A_g^C)^T - (A_g^C)^{th})F_{Cd} \qquad (19)$$

$(A_g^C)^{th}$ is proportional to $(A_g^B)^{th}$ or the thermal activation of a bare foil:

$$(A_g^C)^{th} = X(A_g^B)^{th} \qquad (20)$$

where X is a proportionality factor dependent only on the cadmium thickness. We can rewrite Equation (19):

$$(A_g^B)^{epi-Cd} = ((A_g^C)^T - X(A_g^B)^{th})F_{Cd} \qquad (21)$$

Now since the thermal part of the bare foil activity is the difference between the total bare foil activity and the epicadmium part of the bare foil activity,

$$(A_g^B)^{th} = (A_g^B)^T - (A_g^B)^{epi-Cd} = (A_g^B)^T - [(A_g^C)^T - X(A_g^B)^{th}]F_{Cd} \quad (22)$$

Solving for $(A_g^B)^{th}$, which gives the thermal neutron activation of a bare foil.

$$(A_g^B)^{th} = \frac{(A_g^B)^T - (A_g^C)^T F_{Cd}}{1 - XF_{Cd}} \quad (23)$$

In general for cadmium cover thicknesses of 0. 020 inches or greater the factor X is neglected. Martin (14) says that for a 0. 020 inch thick cadmium cover the value of X is 0. 002. The thickness of the cadmium covers used in this work were approximately 0. 09 inches. Thus the value of X is believed to be extremely small. For 0. 020 inch or thinner cadmium covers the factor X may be important, in particular for high cadmium ratios where $(A_g^B)^T$ is much larger than $(A_g^C)^T$.

Martin (14, p. 10) has experimentally determined a curve of foil saturated activity vs thickness of cadmium covering. The ratio between the relative activity when extrapolated back to zero cadmium thickness and the relative activity at a given cadmium thickness provides the correction factor, F_{Cd}. The value of F_{Cd} for 0. 09 inch thick cadmium covers was found to be 1. 05. This value can be used in Equation 23.

Due to the high thermal neutron flux encountered in the TRIGA, pure gold and manganese foils were not used. Any pure gold or

manganese foil that would be of sufficient thickness for convenient use
would produce activity several orders of magnitude higher than re-
quired when exposed in the high flux regions of the TRIGA. Conse-
quently, gold-aluminum and manganese-aluminum foils containing 0.12
nominal weight percent gold and 0.35 nominal weight percent mangan-
ese respectively were used for thermal neutron flux measurements.
These foils gave adequate activity and were easy to handle.

The self absorption of the manganese 0.85 MeV gamma and the
0.411 MeV gamma of gold will be primarily by the aluminum. Con-
sider that the foil is emitting a total number of S photons per sec-
ond, and that the source is uniformly distributed throughout the foil.
Consider a small increment dx at a distance x from the surface
of the foil. For a foil of thickness t the γ emission of this thin
section is Sdx/t. Consider for a moment that all γ's are emit-
ted so that they leave the foil with a direction that is perpendicular to
the foil face. Thus the γ's emitted by this thin section that reach
the surface of the foil is

$$dA = \frac{Se^{-\mu x}}{t}\, dx \tag{24}$$

where μ is the linear γ attenuation coefficient.

The total γ's reaching the foil surface is

$$A = \frac{S}{t} \int_0^t e^{-\mu x} dx \tag{25}$$

$$A = \frac{S}{\mu t} (1 - e^{-\mu t}) \tag{26}$$

The self absorption factor, F_{SA}, is defined as

$$F_{SA} = \frac{(1 - e^{-\mu t})}{\mu t} \tag{27}$$

The factor μ / ρ (where ρ = density, gm/cm^3) is found from Rockwell (20, p. 448) to be 0.092 cm^2/g for .411 MeV γ's, and 0.067 cm^2/g for .85 MeV γ's. The value of μ for aluminum is thus 0.248 for .411 MeV γ's and 0.181 for .85 MeV γ's. Using a foil thickness, $t = 0.0127$ cm (5 mil foils) we get for gold (.411 MeV γ) - aluminum foils $F_{SA} \cong 1.00$, and for manganese (0.85 MeV γ) - aluminum foils $F_{SA} \cong 1.00$.

The statement that the radiation is emitted perpendicular to the faces (which in effect says that the maximum distance than any γ has to travel to escape the foil is t) is obviously not correct. Yet for 0.411 MeV γ's (worst case) and considering a thickness ten times that of the foils used, F_{SA} is only about 0.99. The problem is in defining the average distance that a γ ray will travel in the foil. Considering the above computations, it is not felt that self absorption in the aluminum foils will be a significant factor.

Consequently no attempt is made to correct for this factor.

The self shielding effect of a detector foil results in the activation of interior points in the foil being less than points near the surface of the detector. In this case all points in the foil are not exposed to a uniform neutron flux. Baumann and Stroud (1) have developed graphs and formulas that simplify the computation of the self shielding factor. They define an activation depression factor F, as the per atom activity of a "thick" foil relative to that for an infinitely thin one. They consider a $1/v$ detector in a Maxwellian beam, and in an isotropic flux. F for a beam of neutrons is

$$F = \frac{1 - e^{-KY_0}}{KY_0} \tag{28}$$

F for an isotropic flux is

$$F = \frac{1 - 2E_3(KY_0)}{2KY_0} \tag{29}$$

where

Y_0 = foil thickness in units of absorption mean free paths

K = factor when multiplied by Y_0 produces the desired effective thickness

E_3 = exponential integral function

Graphs of Y_0 vs. K are given, so K may be found and then KY_0

and hence F. The foils used, as stated previously, are gold-aluminum and manganese-aluminum, containing 99.6 + percent aluminum. Aluminum has a macroscopic cross section for thermal neutrons of 0.014 cm^{-1} as opposed to 5.84 cm^{-1} for gold and 1.083 cm^{-1} for manganese. The value of $\lambda (=1/\Sigma)$ for both types of foils is approximately 50 cm. The foils are 0.0127 cm thick or $2.16 \times 10^{-4} \lambda$, so $Y_0 = 2.16 \times 10^{-4}$; for this small value of Y_0 the value of K is asymptotic to the value $(4/\pi)^{\frac{1}{2}}$ for both the beam and isotropic flux curve so

$$KY_0 = (\frac{4}{\pi})^{\frac{1}{2}} Y_0 = 1.13 Y_0 = 2.75 \times 10^{-4}$$

For a beam F becomes

$$F = \frac{1 - e^{-2.75 \times 10^{-4}}}{2.75 \times 10^{-4}}$$

Expanding the exponential (which is acceptable for very small x, to get $1 - e^{-x} \approx x$) we see that $F \approx 1.0$. For the case of isotropic flux F becomes

$$F = \frac{1 - 2E_3(2.75 \times 10^{-4})}{2(2.75 \times 10^{-4})} \tag{30}$$

Using one of the definitions of exponential integrals we have

$$E_{n+1} = \frac{1}{n-1} [e^{-x} - x E_n(x)] \tag{31}$$

For small x, E_2 approaches 1. Using this and expanding the exponential we get

$$E_3(2.75 \times 10^{-4}) = \frac{1}{2} [1 - (2)(2.75 \times 10^{-4})]$$

Substituting into (30) we get

$$F = \frac{1 - 2(\frac{1}{2})[1 - (2)(2.75 \times 10^{-4})]}{2(2.75 \times 10^{-4})} = 1.0$$

Again F is approximately one. The authors state that these formulas, based on pure absorption, give a good estimation of the self-shielding effects in most detector foils if the scattering cross section is less than the absorption cross section. For manganese and gold this is precisely the case.

The depression of the neutron flux in a diffusing medium has been investigated extensively, both experimentally and analytically (5, 7, 12, 19, 22, 23, 28). In this instance the presence of a strong absorber in the diffusing medium perturbs (depresses) the flux and the foil does not "see" the unperturbed neutron flux, ϕ_0, as shown in Figure 28.

In almost all instances, the foils used for thermal neutron flux measurements in the TRIGA were not exposed in intimate contact with a neutron diffusing medium. In general they were exposed in air

filled cavities of the core, reflector, and thermal column, and in the

beam ports, which are also air filled. It is difficult to think of a foil

causing a "flux depression" in a cavity of the reactor.
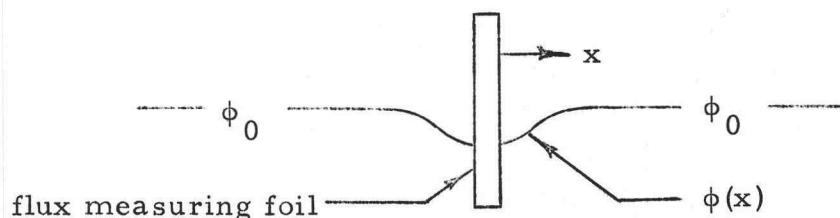
Figure 28.   Flux depression due to a strong absorber in a diffus-
ing medium.

In two instances, however, the foils were exposed in water.

This was in the pool irradiation facility and the central thimble.

While there is a great deal of literature concerning flux depression

factors for pure gold and pure manganese foils of various shapes,

sizes and thicknesses, it is doubtful if any work has been done on alu-

minum alloy foils of the type used in this investigation.   The macro-

scopic absorption cross section of the aluminum alloy foils is approx-

imately the same as for water, e.g. ~ 0.017 cm^{-1}.   It therefore ap-

pears that the foils are not "highly absorbing" in relation to the dif-

fusing medium.   Thus no attempt was made to compute a flux depres-

sion factor for the gold-aluminum and manganese-aluminum foils.

Thermal Neutron Flux Computation

The method for computing saturated activities per gram for irradiated foils is discussed in the Appendix. To determine the thermal neutron flux at a given position in the reactor, a bare foil and a cadmium-covered foil (either gold or manganese) are irradiated simultaneously at the desired position. The foils are counted, and the saturation activity per gram is computed as per the Appendix. Formula 23 is then used to obtain the corrected cadmium difference or the corrected thermal neutron activation of the bare foil. Using Equation A-10 (Appendix):

$$(A_g^B)^{th} = \frac{N_A \sigma \phi_{th}}{M} \tag{32}$$

where

N_A = Avogadro's number $(6.023 \times 10^{23}$ atoms/mole)

M = atomic weight of detector (grams)

σ = thermal neutron cross section, 2200 m/sec value, (cm^2)

ϕ_{th} = thermal neutron flux, $(n/cm^2$-sec)

and solving for ϕ_{th}

$$\phi_{th} = \frac{M(A_g^B)^{th}}{N_A \sigma} \tag{33}$$

We see that the thermal neutron flux is equal to the saturated activity per gram of the bare foil (due to thermal neutrons) times a constant

$M/N_A \sigma$. Using a 2200 m/sec cross section of 13.2 ± 0.1 barns for Mn^{55} and 98.6 ± 0.3 barns for Au^{197} (2, p. 418, 421) the values of the constant are 3.317 ± 0.01 for gold and 6.910 ± 0.05 for manganese.

Discussion of Errors

The parameters that could introduce error of a significant amount into the thermal neutron flux determination are: neutron cross section, foil mass, counter efficiency and statistical error. The errors associated with these factors are discussed below.

The cross sections of Mn and gold are well known. The error listed for the Mn cross section is approximately 0.7 %, while the error for gold is approximately 0.3%.

For a single observation, the standard deviation is given by the square root of the total count, $\sigma = \pm \sqrt{C_3}$. For all foil counting, a total of 10^4 or more counts was obtained. This made the standard error less than or equal to one percent.

The standard gamma sources used to calibrate the counter were reported by the manufacturer to have an error no greater than five percent in the listed activity. Thus it is felt that the error associated with the value of the counter efficiency, ϵ, for a given gamma ray energy, is no greater than five percent.

The error introduced by the foil mass is the most significant. The foils were reported by the manufacturer to contain 0.12 percent

(by weight gold) for the gold-aluminum foils and 0. 35 percent (by

weight manganese) for the manganese-aluminum foils. These per-

centage values were checked by activation analysis. High purity gold

and manganese (of known purity) were dissolved to make solutions of

known concentration. A precise amount of the solution was then ex-

tracted. This was irradiated simultaneously with the foils in the ro-

tary specimen rack. Hence both foils and solution were exposed to

the same neutron flux (the rack was rotating). By determining the

saturated activity of the gold and manganese solutions, and dividing

by the precisely known mass of the gold or manganese present in the

solution, the saturated activity per gram could be determined. Using

this value, and computing the saturated activities of the foils, the

mass of gold or manganese in each foil was determined. The average

gold concentration of the gold-aluminum foils was found to be 0. 16

percent, while the average manganese concentration was found to be

0. 30 percent. These values are significantly (14 to 33 percent) dif-

ferent from the values supplied by the manufacturer. The manufac-

turer was confronted with the anomaly. Additional spectographic and

chemical tests were made on foils from the same lot as ours by the

manufacturer. These tests gave the following results: .14 percent

by weight gold, in the gold-aluminum foils; 0. 33 and 0. 34 percent by

weight manganese in the manganese-aluminum foils. The standard

error associated with the gold concentration (three values) is 14

percent. The standard error associated with the manganese concentration (four values) is nine percent.

The gold and manganese mass values determined by irradiation were used in all computations of thermal neutron flux, as opposed to those quoted by the manufacturer. This procedure, in general, results in conservative flux values being quoted. The error associated with using these mass values is on the order of 14 percent for gold foil computions.

The overall error associated thermal neutron fluxes quotes is approximately ± 20 percent. Perhaps a quotation of + 20 percent, - 6 percent would be more significant in light of the mass values used.

Fast Neutron Spectrum Measurements

Threshold Detectors

Some of the more common techniques utilized for fast neutron spectrum measurements are: particle recoil, photographic emulsions, and threshold detectors. Threshold detectors are attractive from the standpoint of gamma-ray insensitivity, small size, and low cost, and they require only standard beta and gamma radiation detectors for obtaining data.

In the case of some neutron-induced reactions, the energy of the neutron precipitating the reaction must be above a certain value,

called the threshold energy, before the reaction can be initiated. Reactions and materials that exhibit these reactions are called threshold reactions and detectors. In the neutron energy range of a nuclear reactor there are two principal reactions of interest: (n, p) and (n, α) reactions. These two reactions are represented as

$$A(n, p)B$$

and (34)

$$C(n, α)D$$
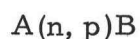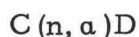
where

A, C = target nucleus (threshold detector)

n = incident neutron

p, α = emitted particle, (proton and α-particle respectively)

B, D = residual nucleus

(n, p), (n,α) = threshold reaction

Some materials, such as aluminum, undergo both reactions in the neutron energy range of interest. The residual nucleus, B and D above, is radioactive and emits γ-rays and/or β particles. A radioactivant that emits a γ-ray can be counted in a scintillation detector, while a pure β emitter may be counted with a Geiger-Mueller or proportional counter.

If several detectors, each with a different threshold energy, are exposed to a neutron flux, it is possible, in theory, to obtain

information about the neutron energy spectrum. Knowing the cross

section, the integral flux above the threshold energy may be deter-

mined from experimental activation of the detector. The average

flux between any two energy thresholds may be obtained by subtrac-

tion. In this manner, a histogram-type spectral representation can

be generated. The energy resolution of the spectrum would be depend-

ent upon the number of detectors used.

The cross section of an ideal threshold detector would have a

energy variation as follows:

$$\sigma(E) = 0 \qquad\qquad 0 < E < E_T$$
$$\sigma(E) = \text{constant} \qquad E_T < E < \infty$$

(35)

This ideal cross section variation is shown in Figure 29.
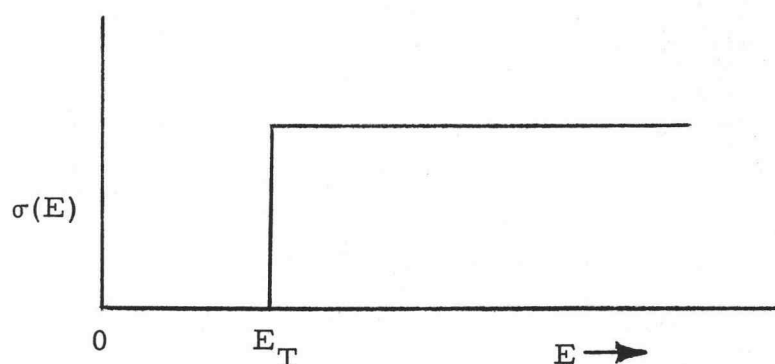
Figure 29. Cross section variation of an ideal threshold de-
tector.

Unfortunately, no threshold detector exhibits this ideal cross

section dependence. The cross sections of some important

threshold detectors are shown in Figure 30. It can be seen from

Figure 30, that only σ_f for U^{238} approximates the ideal step func-

tion threshold cross section. It is the irregular energy dependence

of the threshold cross sections that accounts for the difficulty in ob-

taining good spectral information from radioactivant measurements.

Methods of Analysis

The primary data obtained from threshold detectors are the

activities of the product isotopes resulting from the reactions of in-

terest. These are reduced to saturated activities of the radioacti-

vants by a method discussed in the Appendix. The relation between

saturated activity and neutron flux for a particular radioactivant, i,

may be expressed as

$$A_{si} = (C.F.) \times N_i \int_0^\infty \sigma_i(E)\phi(E)dE \qquad (36)$$

where

A_{si} = saturated activity of the ith radioactivant (sec^{-1})

N_i = number of target atoms

$\phi(E)$ = neutron flux ($cm^{-2}sec^{-1}$)

$\sigma(E)$ = reaction cross section (cm^2)

(C.F.) = correction factors, as per Appendix

There are a number of methods available for using radioactivant
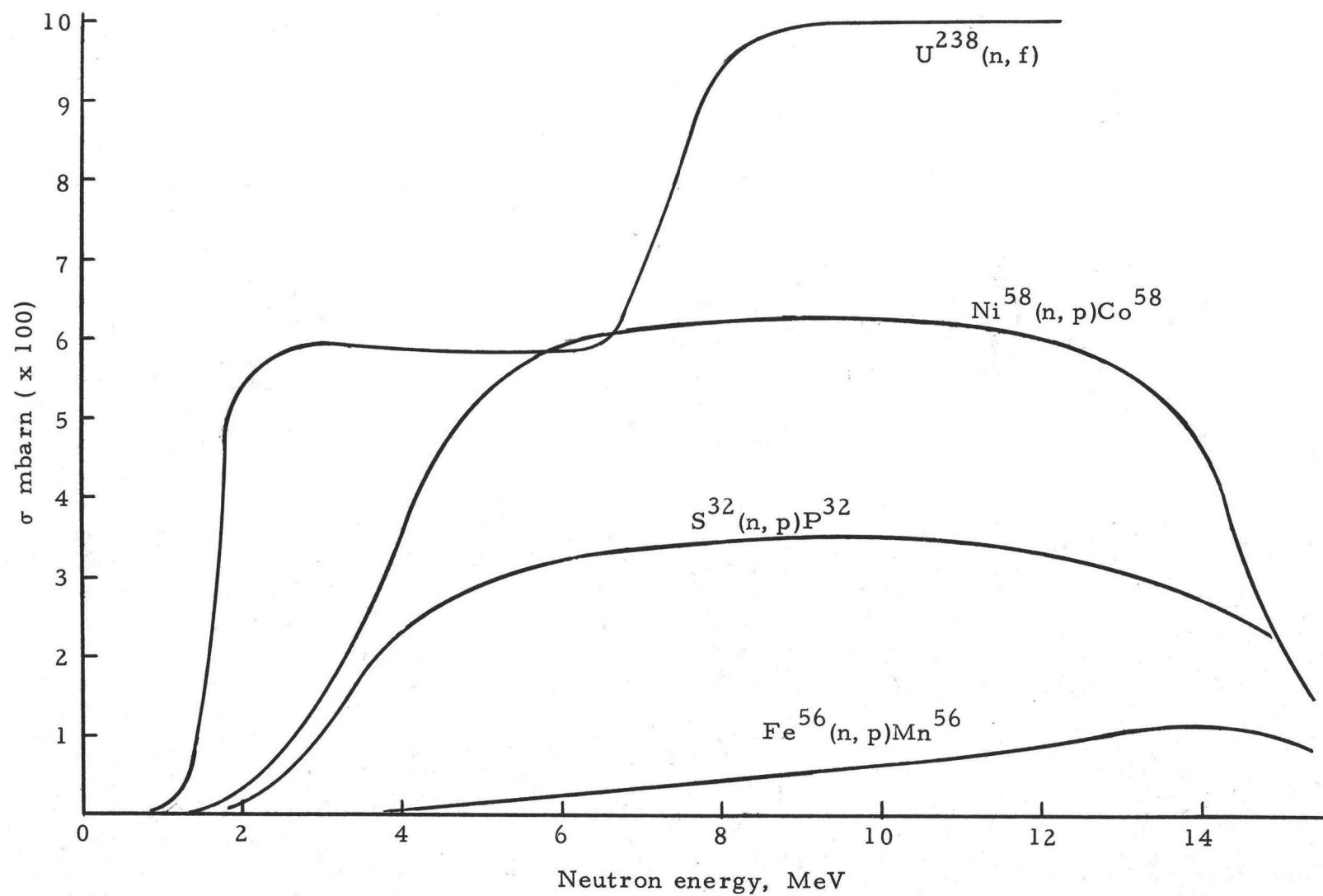
Figure 30.   Cross sections for various threshold detectors.

data to obtain flux spectra. Most of the methods assume a spectral shape with unspecified coefficients. The cross section data are integrated over an energy interval with respect to the assumed spectral shape, and then the experimentally determined activations are used to determine the appropriate coefficients of the assumed shape, thus specifying the measured spectrum. All of the available method require an accurate knowledge of the neutron cross section for the reactions of interest.

A brief listing of some of the methods proposed for extracting neutron spectra is given below. No attempt is made to explain the theory of each method, nor the advantages and disadvantages inherent in each. The listing is primarily a reference for the reader desiring to pursue this subject matter more extensively. Some of the methods available are: the flux integral method (8, p. 98), the Dierckx method (27, p. 7), the iterative method (27, p. 9), the polygonal method (18, p. 117), the orthonormal method (16, p. 135), the orthonormal-polynominal method (18, p. 150) and empirical methods (27, p. 20).

The flux integral, or effective threshold method (27, p. 6) was selected for analysis of the activation data. It is the oldest and most widely used method of analyzing radioactivant data. In this method the actual reaction cross section is replaced by an idealized step-function cross section. Thus Equation 36 becomes:

$$A_{si} = N_i \int_0^\infty \sigma_i(E)\phi(E)dE = N_i\sigma_{i \text{ eff}} \int_{E_{eff}}^\infty \phi(E)dE \qquad (37)$$

Define

$$\phi_{i \text{ eff}} = \int_{E_{eff}}^\infty \phi(E)dE \qquad (38)$$

then

$$\phi_{i_{eff}} = \frac{A_{si}}{N_i\sigma_{i \text{ eff}}} \qquad (39)$$

where

$\sigma_{i \text{ eff}}$ = the effective cross section for the reaction (cm^2)

ϕ_{eff} = the integral flux above the effective threshold energy,

   E_{eff} $(cm^{-2}sec^{-1})$

By using several detectors, a histogram plot of the intergral flux may be determined. To determine the effective cross section and effective threshold energy, a neutron spectrum is assumed. Generally the assumed spectrum is a fission spectrum (Watt (24) or Cranberg (4)). $\phi(E)$ is replaced by this in Equation (37); the first integral in Equation (37) can then be numerically integrated. By using the chosen value of σ_{eff} and the fission spectrum, the second integral in Equation (37) is numerically evaluated. A value of E_{eff} is chosen so that this quantity numerically equals the first integral. If the measured spectrum differs appreciably from the spectral form used to determine σ_{eff} and E_{eff}, an error will be introduced.

Experimental Techniques

Threshold detectors were chosen on the basis of threshold energy, half-life, and physical and chemical properties. Detectors with thresholds greater than 1 MeV were examined and selected to give a fairly uniform distribution of energies in the range of interest (1 to 8 MeV). The threshold reactions selected appear in Table 2. Very pure foils of aluminum, titanium, nickel and iron were obtained. Sulfur pellets and uranium foils (natural) depleted to 378 parts per million U^{235} were also obtained. It became evident early in this investigation that the sulfur pellets would be unsatisfactory for use as a threshold detector without additional counting techniques. The P^{32} formed from the S^{32} (n, p) P^{32} reaction emits no gamma ray (only a 1.71 MeV β). The self absorption of the P^{32} β particles in the large (3/16 inch thick) sulfur pellets is very high, and difficult to estimate. Usually the sulfur is "burned off," leaving only the radioactive P^{32}. This method is considered too elaborate. Thus the sulfur was not used as a threshold detector. The (n, p) reaction of N_i^{58} has approximately the same threshold as S^{32} (n, p) P^{32}, and was used in place of the sulfur.

The depleted uranium foils, essentially pure U^{238}, undergo fission, and a specific fission product must be counted to enable absolute flux determination. The 1.60 MeV γ-ray of La^{140} was chosen

Table 2. Threshold detector properties.

Reaction	E_{eff}, effective threshold energy MeV	σ_f, cross section for a fission spectrum millibarns	Disintegration particle or photon energy MeV	Halflife
$U^{238}(n, f)$	1.67	310	1.60 (La^{140})	$Ba^{140} \xrightarrow{12.8d} La^{140} \xrightarrow{40.2h}$
$Ni^{58}(n, p)Co^{58}$	3.1	101	.81	71.3d
$S^{32}(n, p)P^{32}$	3.2	54	1.71 (β)	14.5d
$Ti^{47}(n, p)Sc^{47}$	3.7	16	.16	3.4d
$Fe^{54}(n, p)Mn^{54}$	3.75	60	.842	300 d
$Al^{27}(n, p)Mg^{27}$	4.6	3.5	.843	9.5m
$Ti^{46}(n, p)Sc^{46}$	5.5	9.1	1.12	85 d
$Fe^{56}(n, p)Mn^{56}$	6.4	.87	.845	2.58h
$Ti^{48}(n, p)Sc^{48}$	7.2	.5	1.040	44 h
$Al^{27}(n, \alpha)Na^{24}$	8.1	.57	1.368	15.0h

because of its prominence in the fission product spectrum at the time of counting. The maximum La^{140} activity occurs about seven to eight days after irradiation, and the fission foils were counted at this time.

All of the threshold foils were irradiated with cadmium covers to minimize thermal neutron activation of the detector materials.

The threshold detectors were irradiated in sets (U, Ni, Ti, Al, Fe) in the rabbit, the rotating rack, and the central thimble. It was believed that the neutron spectrum would be sufficiently similar to a fission spectrum in these in-core and near-core facilities.

The counting procedure used to count the threshold foils is outlined in the section on foil counting. The computation of saturated activity is outlined in the Appendix. The integral flux was computed for each reaction by dividing the saturated activity by the appropriate constants, including the effective cross section.

The effective cross section and effective threshold energy values used are listed in Table 2. These values were obtained from the literature, and represent the most frequently quoted values, as there is great variation in cross section values quoted for some threshold reactions. The cross section and effective threshold are those for a fission neutron spectrum.

As stated previously, by using several detectors, a histogram plot of the integral flux may be determined. Alternately, a smooth

curve may be drawn through the integral flux data and the curve differentiated to obtain the differential flux. This procedure, of graphical differentiation, is a difficult problem in graph analysis and the accuracy of the differential flux curve would probably not warrant the effort expended. Consequently, the results of the fast neutron spectra measurements are shown (Figures 7, 9 and 12) as integral flux measurements. A flux value shown for a given energy, E, is:

$$\phi_E = \int_E^\infty \phi(E)dE \tag{40}$$

ϕ_E = total neutron flux above energy E. $cm^{-2}sec^{-1}$

Also shown in Figures 7, 9 and 12 are integral flux values derived from the fission neutron spectrum. The mathematical expression used to represent the fission neutron spectrum is integrated using a computer code utilizing Simpson's numerical integration formula. This is done for all of the energies of the effective thresholds. The integral flux above 1.67 MeV (the effective threshold for U^{238} (n, f)) is computed thusly

$$\phi_{1.67} = \int_{1.67}^{17} \sinh (2.29E)^{\frac{1}{2}} e^{-1.036E} dE \tag{41}$$

This expression for the fission neutron spectrum is reported to be valid up to 17 MeV. The value computed from Equation (41) is

normalized to the experimentally determined integral flux vlaue for

U^{238}. A plot of the relative fission integral neutron flux is obtained

by replacing the lower limit of the integral in Equation (41) by the en-

ergy of the various threshold reactions.

Discussion of Results

The integral neutron flux measurements are shown in Figures

7, 9 and 12. The agreement with the curve calculated from the fis-

sion neutron spectrum is within a factor of three at the higher neutron

energies. Not all of the threshold reactions were used as data points

for the experimental curves. The flux values computed from some

of the threshold detectors did not give a good fit to the curve (gener-

ally gave values greater than the curve). The reactions that were

not acceptable are $Ni^{58}(n, p)Co^{58}$, and $Fe^{56}(n, p)Mn^{56}$. Those reac-

tions that gave limited success are $Al^{27}(n, a)Na^{24}$ and $Ti^{46}(n, p)Sc^{46}$.

The errors introduced in these foil measurements are associ-

ated with counting, weighing, half life, isotopic abundance, and cross

section errors. Of the above errors, the uncertainty in cross is by

far and away the source of largest error. Estimates of the uncer-

tainty in published cross section data, range in value from ± 5 to ± 50

percent.

Another consideration is that an undegraded fission neutron

spectrum may not be present at the facilities where the spectrum

measurements were made. The central thimble is in the center of the core, and is water filled, the rabbit is outside the active (fuel region) core, and the rotating rack is located within the graphite reflector. The central thimble fast neutron spectrum should more closely approximate a fission neutron spectrum than the rabbit or the rotating rack, yet the agreement between the experimental and calculated results for the central thimble is approximately the same as that for the rabbit and rotating rack.

The fact that some reactions did not give good results is probably due to inaccuracies in the cross section values for these reactions. The lack of agreement between the experimental results and the calculated curves are probably due to the use of the Effective Threshold Method. This method assumes a fission spectrum and uses cross sections and effective thresholds applicable to a fission spectrum. The assumption of a fission neutron spectrum in the facilities where the threshold detectors were used may be somewhat in error.

<center>Foil Counting</center>

Counting Equipment

The induced activity present in foils used for fast neutron and thermal neutron measurements was counted with a NaI(Tl) scintillation crystal in conjunction with a 400-channel differential pulse-height

analyzer.

The NaI(Tl) scintillation crystal is a 3 inch x 3 inch cylindrical crystal with a two inch deep well. Samples are placed in polyethylene capsules and then placed in the well of the crystal. The well crystal is optically coupled to a photomultiplier tube. The crystal/photomultiplier tube combination are housed in a two inch thick lead cave.

The output from the detector is sent to a linear pulse height amplifier incorporated into the pulse-height analyzer (PHA), the gain of the PHA is set so that each channel is ten KeV wide. The γ-ray energy span is then approximately .05 MeV to 4.00 MeV.

The γ rays from the radioactive foil interact and deposit their energy in the NaI(Tl) crystal. This energy is released in the crystal as a light pluse, or scintillation. The light pulses emitted by the scintillation crystal are proportional to the energy deposited in the crystal by the γ ray. These pulses are collected and stored in a PHA and are displayed as the number of pulses of a given height vs pulse height. This display forms a γ-ray spectrum. Since the pulse height is proportional to the γ-ray energy, a plot of counts vs energy is obtained.

Gamma-Ray Interactions

Gamma rays interact in a NaI(Tl) crystal in primarily three ways: the photoelectric effect, the Compton effect, and pair production. All three of these processes produce secondary electrons

which deposit their energy in the crystal and produce the scintillations. In the γ-ray energy range of interest (0.4 to 3.0 MeV) the Compton effect is the dominant contributor to the absorption coefficient of NaI. The Compton effect involves the interaction of the γ ray and a free electron; the γ ray gives some of its energy to the electron, and it may then interact again by the Compton effect or the photoelectric effect. Usually one of the scattered γ rays (from the first, second, ... or nth Compton interaction of the primary γ ray) will escape from the crystal, and a pulse will appear in the spectrum at an energy below the photopeak (or incident γ-ray) energy. These pulses can appear at any fraction of the incident γ-ray energy, depending upon the scattering angle. A great number of γ rays interacting in this manner gives rise to a continuous distribution of pulses, having about the same number of pulses at each energy, from the incident γ-ray energy down to essentially zero energy. The continuous Compton distribution is shown in Figure 31. Also shown in Figure 31 is the backscatter peak. This results from the incident γ ray undergoing a large-angle Compton scattering from the shield walls, then entering the crystal and depositing its remaining energy.

Analysis of Gamma-Ray Spectra

There exist a number of sophisticated methods for analyzing gamma ray spectra. These include spectrum stripping, spectrum
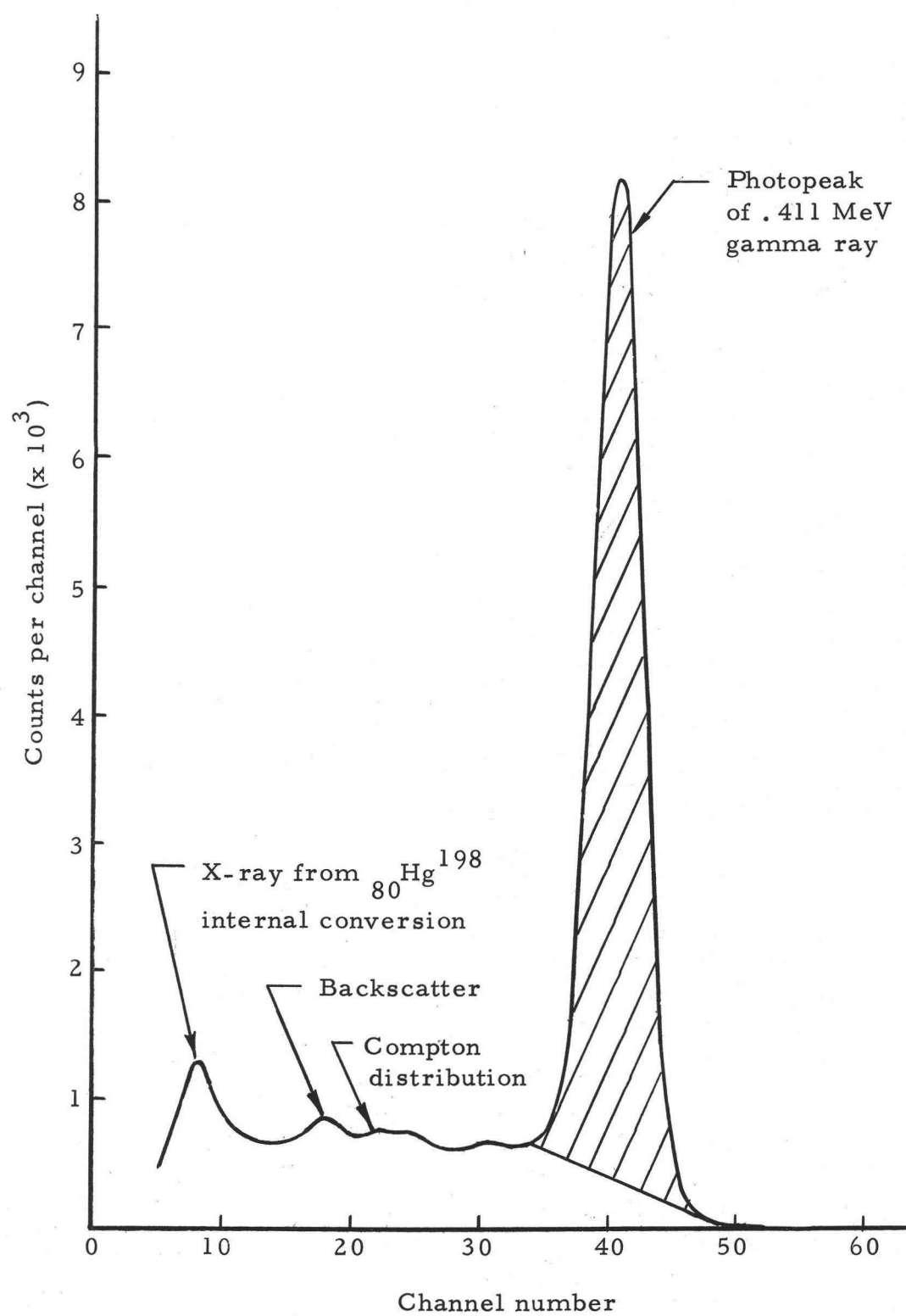
Figure 31.   Gamma-ray spectrum of Au^{198} showing net photo-
peak area.

unfolding, and least-squares analysis. All of the γ-ray spectra encountered in this work were relatively simple; usually containing a single photo peak. The above methods are generally used to analyze complex spectra containing many peaks.

A simple and easily reproducible method was used to find the photopeak area. The integral of the total counts in the photopeak was taken on the 400-channel analyzer. From this, the Compton background was subtracted, giving a net photopeak area. This procedure is shown in Figure 31, the cross-hatched region denotes the net photopeak area. The exact Compton background to be subtracted from the total photopeak count is somewhat subjective, and can introduce error into the computation of the actual, net photopeak count.

Counter Calibration

The gamma-ray calibration of the well crystal utilized the above technique. The efficiency of the well crystal was determined for various energies by using calibrated gamma reference sources of known disintegration rate. The net photopeak efficiency vs. energy for the well crystal is shown in Figure 32. The calibrated sources are held in a plastic rod, 1/4 inch from one end. The rod is then positioned in the well of the crystal, with the activity near the botton of the well. The sources used are listed in Table 3.
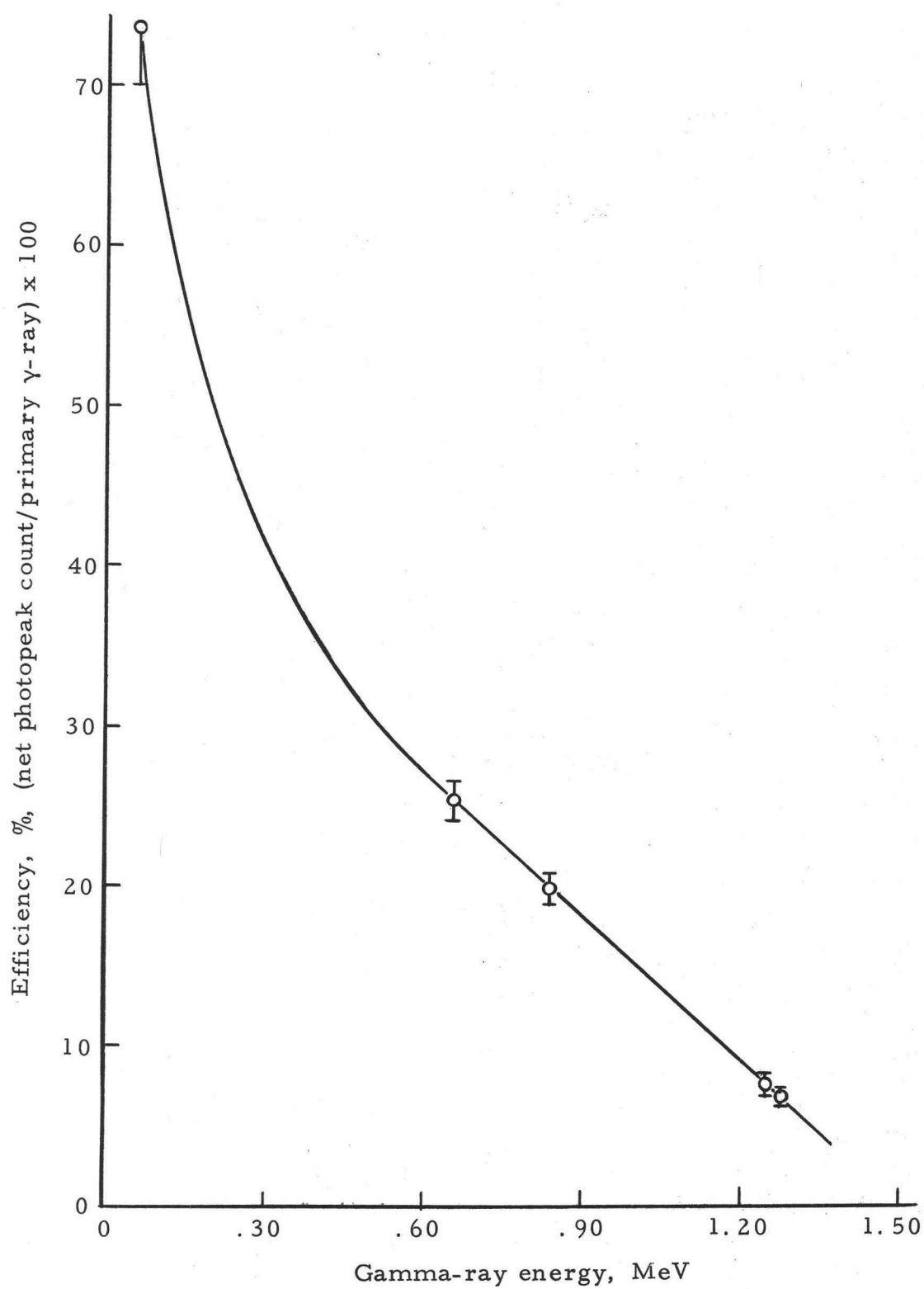
Figure 32.   Efficiency of NaI(Tl) well crystal.

Table 3.   Gamma ray sources used for calibra-
tion of well crystal.

Source	Principal gamma-ray energy, MeV
Co^{57}	.136
Cs^{137}	.662
Mn^{54}	.835
Na^{22}	1.28
Co^{60}	1.17, 1.33

The calibration of the well crystal in terms of net photopeak

efficiency is in keeping with the method of foil counting.   The net

photopeak area is determined from counting a foil, this value is di-

vided by the efficiency (defined as net photopeak counts/gamma-ray

emitted) to find the actual emission rate of the γ-ray of interest.

The emission rate of the primary γ-ray may be related to the actual

disintegration rate through the branching ratio, as defined in the Ap-

pendix.

CONCLUSIONS AND RECOMMENDATIONS

Gamma-ray and neutron fluxes have been measured in the experimental facilities of the Oregon State TRIGA reactor. Results have been reported for each facility, providing future experimenters with information on neutron and gamma fluxes in a given facility.

The gamma-ray dose measurements utilized a thermoluminescent dosimetry system. The thermoluminescent material used was LiF. This dosimetry system is very attractive from the standpoint of the wide range of doses it can measure. The dosimeters are reusable and of a small size. Care must be taken, however, when measuring gamma doses in a mixed radiation field (γ + neutron) with LiF dosimeters. The dosimeters were found to be thermal neutron sensitive, and consequently were irradiated in cadmium covers to shield out the thermal neutrons. The effect of fast neutrons on LiF is not as well known, and should be researched more extensively to specify what contribution, if any, the fast neutron exposure has on LiF dosimeters. The experimental error associated with the gamma-ray dose measurements is on the order of $\pm$ 15 percent.

The thermal neutron flux and cadmium ratio were measured with foil activation techniques. The foils were counted with a NaI(Tl) scintillation crystal, calibrated with gamma-ray sources of known source strength. This method is very convenient, and requires

a minimum of investment in equipment. Once the experimental procedure is well defined the flux measurements can be rapidly performed. The largest source of error in the thermal neutron flux measurements was introduced by the uncertainty in the mass of gold and manganese present in the aluminum alloy foils. The mass value chosen for computational use resulted in conservative flux values being quoted. The experimental error associated with the thermal neutron flux measurements is on the order of $\pm$ 20 percent.

Measurement of the fast neutron spectrum using threshold detectors was also accomplished in the in-core and near-core facilities. The threshold detectors were chosen to cover the energy range of interest (2 to 8 MeV). Some of the threshold reactions used did not give consistent results. This may be due to inaccuracies in the cross section values used. The method used to generate a neutron spectrum from the activity data obtained from the threshold detectors is the Effective Threshold Method. The main disadvantage of this method is that a neutron spectrum form must be assumed in order to generate cross sections and effective threshold values. The spectrum usually assumed is a fission neutron spectrum. If the measured spectrum differs appreciably from the spectral form used to determine the cross section and the effective threshold for the threshold reaction, an error will be introduced. The agreement between the experimentally measured neutron spectrum and the fission neutron

spectrum is within a factor of three at high neutron energies (worst case). It is recommended that more sophisticated techniques, not requiring a prior knowledge of the neutron spectrum, be considered for future spectral measurements.

BIBLIOGRAPHY

1. Baumann, N. P. and M. B. Stroud. Self shielding of detector foils in reactor fluxes. Nucleonics 23:98-100. 1965.

2. Beckurts, K. H. and K. Wirtz. Neutron physics. New York, Springer-Verlag, 1964. 444 p.

3. Cameron, J. R. et al. Thermoluminescent radiation dosimetry utilizing LiF. Health Physics 10:25-29. 1964.

4. Cranberg, L. et al. Fission neutron spectrum of U^{235}. Physical Review 103:662-667. 1956.

5. Dalton, G. R. and R. K. Osborn. Flux perturbations by thermal neutron detectors. Nuclear Science and Engineering 9:198-210. 1961.

6. Evans, R. D. The atomic nucleus. New York, McGraw-Hill, 1955. 972 p.

7. Hanna, G. C. The depression of thermal neutron flux and density by absorbing foils. Nuclear Science and Engineering 11:338-339. 1961.

8. Hughes, D. J. Pile neutron research. Cambridge, Mass., Addison Wesley, 1953. 368 p.

9. Hughes, Donald J. and Robert B. Schwartz. Neutron cross sections. 2d ed. Brookhaven National Laboratory, 1958. 373 p. (U. S. Atomic Energy Commission. BNL-325)

10. Kastner, Jacob, B. G. Oltmann and Pete Tedeschi. LiF thermoluminescent response to fast neutrons. Health Physics 12:1125-1128. 1966.

11. Kastner, Jacob et al. The effects of fast neutron exposure on the $Li^{7}F$ thermoluminescent response to gamma rays. Health Physics 13:918-919. 1967.

12. Klema, E. D. and R. H. Ritchie. Thermal neutron flux measurements in graphite using gold and indium foils. Physical Review 87:167. July 1952.

13. Lederer, C. M., J. M. Hollander and Isadore Perlman. Table of isotopes. 6th ed. New York, John Wiley, 1967. 594 p.

14. Martin, David H. Correction factors for measurements with cadmium covered foils. Oct. 1954. 13 p. (U. S. Atomic Energy Commission. NAA-SR-1076)

15. Morehead, F. T. and F. Daniels. Thermoluminescence and coloration of lithium fluoride produced by alpha particles, electrons, gamma-rays and neutrons. Journal of Chemical Physics 27: 1318. 1957.

16. Marrone, M. J. and F. H. Attix. Damage effects in CaF_2: Mn and LiF thermoluminescent dosimeters. Health Physics 10:431-436. 1964.

17. Prince, J. R., Instructor, Health Physics Department, Radiation Center, Oregon State University. Personal communication. Corvallis, Oregon. Dec. 2, 1967.

18. Ringle, John C. A technique for measuring neutron spectra in the range 2.5 to 30 MeV using threshold detectors. PhD. thesis. Berkeley, University of California, 1963. 221 numb. leaves.

19. Ritchie, R. H. and H. B. Eldridge. Thermal neutron flux depression by absorbing foils. Nuclear Science and Engineering 8:300-301. 1960.

20. Rockwell, Theodore, ed. Reactor shielding design manual. New York, D. Van Nostrand, 1956. 472 p.

21. Simpson, R. E. The response of lithium fluoride to reactor neutrons. Nuclear Applications 3:500-506. 1967.

22. Sola, Alain. Flux, perturbation by detector foils. Nucleonics 18:78-80. 1960.

23. Tittle, C. W. Slow neutron detection by foils. Nucleonics 8:5. 1951.

24. Watt, B. E. Energy spectrum of neutrons emitted from thermal fission of U^{235}. Physical Review 87:1037-1041. 1952.

25. Westcott, C.H. Effective cross section values for well moderated thermal reactor spectra. Nov. 1960. 37 p. (U.S. Atomic Energy Commission. AECL-1101)

26. Westcott, C.H. The specification of neutron flux and nuclear cross sections in reactor calculations. Journal of Nuclear Energy 2:59. 1955.

27. Wood, R.J. Fast neutron spectrum measurements by radioactivant techniques. Master's thesis. Seattle, University of Washington, 1965. 26 numb. leaves.

28. Zobel, W. Experimental determination of corrections to the neutron activation of gold foils in water. Oak Ridge National Laboratory, April 1963. 64 p. (U.S. Atomic Energy Commission. ORNL-3407)

APPENDIX

Computation of Saturated Activity

When a foil is irradiated in a neutron flux the differential equation describing the time rate of change of the radioactive nuclide (N_1) is:

$$\frac{dN_1}{dt} = N\sigma_a\phi - \lambda N_1 \qquad (A-1)$$

where

N = number of target atoms in the foil

N_1 = number of atoms of the radioactive nuclide

σ_a = absorption cross section of target atoms for neutrons of energies present (cm^2)

ϕ = neutron flux $(cm^{-2}sec^{-1})$

λ = decay constant of radioactive nuclide (sec^{-1})

The solution to the above equation is

$$N_1(t) = \frac{N\sigma_a\phi}{\lambda}(1-e^{-\lambda t}) \qquad (A-2)$$

The activity of the radioactive atoms (A_1) is given by the decay constant (λ) times the number of atoms present (N_1). Hence the activity for an irradiation time of t_r(sec.) is given by:

$$A_1 = N\sigma_a\phi(1-e^{-\lambda t_r}) \qquad (A-3)$$

If the foils are delayed a certain time before counting begins the activity at the end of this waiting time is:

$$A_2 = A_1 e^{-\lambda t_w} \qquad \text{(A-4)}$$

where

t_w = wait time = time between end of irradiation time and beginning of count time (sec).

As the foils are being counted, they are also decaying. Thus for a count time of t_c, the total number of counts recorded is:

$$C_3 = k\epsilon \int_0^{t_c} A_2 e^{-\lambda t} dt = \frac{k\epsilon A_2}{\lambda} (1 - e^{-\lambda t_c}) \qquad \text{(A-5)}$$

where

ϵ = counter efficiency for the photon being counted (counts/photon)

k = fraction that photon being counted is given off per disintegration of radioactive atom (photon/disintegration)

Thus,

$$C_3 = \frac{k\epsilon N\sigma_a \phi}{\lambda} (1 - e^{-\lambda t_r}) e^{-\lambda t_w} (1 - e^{-\lambda t_c}) \qquad \text{(A-6)}$$

The saturated activity is defined as:

$$A_s = N\sigma_a\phi \quad (\sec^{-1}) \tag{A-7}$$

The saturated activity per gram is defined as:

$$A_g = \frac{A_s}{m} = \frac{N\sigma_a\phi}{m} \tag{A-8}$$

where

  m = mass of target atoms in foil (grams)

Since

$$N = \frac{N_A m}{M} \tag{A-9}$$

where

  N_A = Avogadro's number (atoms/mole)

  M = atomic weight of detector material (grams/mole)

We can also write

$$A_g = \frac{A_s}{m} = \frac{N\sigma_a\phi}{m} = \frac{N_A \not{m}\sigma\phi}{M\not{m}} = \frac{N_A \sigma\phi}{M} \tag{A-10}$$

A short computer program was written to compute the quality $A_g \epsilon k$ from the input parameters $t_c, t_r, t_w, m, C_3,$ and halflife. This value was then divided by ϵk to get A_g. The code along with a sample data input is listed below:

```
$ JOB, 75217NEWT, UPHAM,    , NEUTRON
$ FORTRAN, L, X
        PROGRAM NEUTRON
C       THIS IS A PROGRAM TO COMPUTE SATURATION
C       ACTIVITY PER GRAM.
10      READ(60, 100)C3, TW, TR, TC, HALFLIFE, XMASS
        60 TO(105, 20)EOFCKF(60)
20      XLAMBDA = ALOG(2. 0)/HALFLIFE
        X = -XLAMBDA*(60. 0*TR)
        Y = -XLAMBDA*(60. 0*TC)
        Z = -XLAMBDA*(60. 0*TW)
        ASAT = XLAMBDA*C3/((1. 0-EXP(X))*(EXP(Z))*(1. 0-EXP(Y))
        ASAT = ASAT/XMASS
        WRITE(61, 101)ASAT
        GO TO 10
100     FORMAT(E12. 5, F8. 3, 2F5. 3, 2E12. 5)
101     FORMAT(E12. 5)
105   · STOP
        END
          FINIS
$ LOAD, 56
$ RUN,
+9. 95800E+03099350002500004430+2. 33280E+05+5. 6334-E- 05
```

The units of t_w, t_c and t_r are minutes. The halflife is in seconds, m has units of grams, and C_3 is the counts, corrected by subtracting the background counts from the total counts.

Counter Efficiency

The factor ϵ represents the photopeak efficiency of the 3" x 3" NaI(Tl) well crystal for the photon being counted. This factor is obtained from Figure 32.

k Factor

The factor k accounts for the fact that for some radioactive substances every disintegration of a radioactive nuclide does not result in the photon of interest (the specific photon being counted) being emitted. The decay scheme of Au^{198} (formed by neutron capture from Au^{197}) illustrates this (13, p. 383)
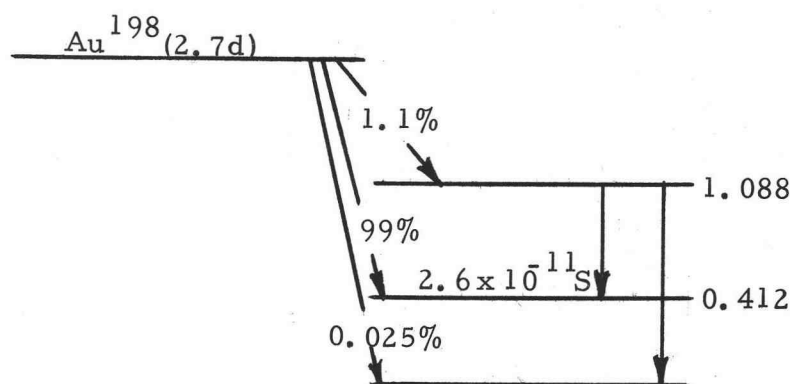
Figure 33. Au^{198} decay scheme.

in 98.88 percent of the disintegrations the Au^{198} nucleus emits a 0.96 (max) MeV beta particle. Of the two possible decay modes from 1.088 MeV, the 1.088 MeV gamma is emitted ~ 19% of the time.

The 0.676 gamma is emitted ~ 81%. Hence the total percent of dis-integrations resulting in the production of the daughter nucleus $_{80}Hg^{198}$ in an excited level which is 0.41 MeV about the ground level is 99.77% (98.88 + (1.1)(0.81)). About 95.6 percent of these excited nuclei go to ground level by emitting 0.411 MeV gamma ray. The others go to ground level by internal conversion, 3 percent in the K shell, 1.1 percent in the L shell, and 0.3 percent in the M shell (6, p. 24).

Thus the factor k for Au^{198} is 0.954 (obtained from 0.9977 x 0.9560). The factor k for Mn^{56} obtained in a similar manner is 0.99.